

Interaction of Nanomaterials with Biological Systems: From Inhalation of Multi-Walled Carbon
Nanotubes to the Treatment of Kidney Stones

by

Judith Dominguez

Department of Mechanical Engineering and Materials Science
Duke University

Defense Date: December 12, 2024

Approved:

Christine K. Payne, Supervisor

James Bonner

Pei Zhong

Mark Walters

Dissertation submitted in partial fulfillment of the requirements for the degree of Doctor of
Philosophy in the Department of Mechanical Engineering and Materials Science in The Graduate
School of
Duke University
2024

ABSTRACT

Interaction of Nanomaterials with Biological Systems: From Inhalation of Multi-Walled Carbon
Nanotubes to the Treatment of Kidney Stones

by

Judith Dominguez

Department of Mechanical Engineering and Materials Science
Duke University

Defense Date: December 12, 2024

Approved:

Christine K. Payne, Supervisor

James Bonner

Pei Zhong

Mark Walters

An abstract of a dissertation submitted in partial fulfillment of the requirements for the degree of
Doctor of Philosophy in the Department of Mechanical Engineering and Materials Science in The
Graduate School of
Duke University
2024

Copyright by
Judith Dominguez
2024

Abstract

Nanomaterials are widely used in the electronics, automotive, medical, and industries. As usage increases, we need to better understand the health effects of human exposure to these unique nanomaterials. Multi-walled carbon nanotubes (MWCNTs) are nanomaterials that are becoming increasingly common in next-generation technologies. Occupational inhalation of MWCNTs, is of particular concern. The high surface area per unit mass of MWCNTs provides a relatively large surface area for protein adsorption. The resulting protein “corona” dictates the subsequent biological response to these nanomaterials. Our goal is to understand how MWCNTs interact with the protein environment of the lung including bronchoalveolar lung fluid (BALF), albumin, which is the most abundant protein present in BALF, and inhaled allergens. House dust mite (HDM) allergens, known to trigger of allergic airway diseases, particularly asthma, are of specific interest. The coronas formed by these biomolecules were characterized for individual proteins and proteins in combination. We found that der p 2, a protein associated with human allergic responses to HDM, dominates the composition of coronas following subsequent exposures to lung fluid proteins.

To better understand the biological implications of HDM adsorption on MWCNTs (HDM-MWCNT), we evaluated the proteolytic activity of the allergens found in interactions between HDM and MWCNTs. HDM contains cysteine and serine proteases, enzymes that break down protein, that contribute to the pathophysiology of

allergic airway diseases when active. We compared the active enzyme activity in free HDM, a mixture of HDM and MWCNTs, and HDM-MWCNT. We also compared the active enzyme concentration of trypsin and papain coronas on MWCNTs and polystyrene nanoparticles (PS NPs). The results should that proteases adsorbed on to the surface of the nanomaterial are less active than in free enzymes. This suggests the activity of proteases is inhibited when adsorbed onto MWCNTs and PS NPs compared to the activity of free proteases.

Interactions between lung fluid proteins and MWCNTs was further investigated by measuring the concentration of albumin, as representative protein for lung fluid, on the surface of pristine, purified and functionalized MWCNTs. In order to understand how MWCNT compositional and surface modifications can affect the protein corona, we measured the concentration of albumin protein coronas as a function of initial albumin concentration. We found that each type of MWCNT displayed a different relationship between the concentration of the protein corona and the initial concentration. This implies that MWCNT purification and functionalization affect the interactions between lung fluid proteins and MWCNTs.

Nanomaterials also have potential to advance medical treatments. In this work, we aim to characterize an ITO@SiO₂ nanofluid to mitigate thermal damage to surrounding tissues during kidney stone laser lithotripsy treatment. We characterized the stability of ITO@SiO₂ in solution and after being exposed to extreme laser pulses. The NPs were unharmed after laser treatment. This was proven by measuring the

concentrations of tin and indium in the supernatant. There were no significant traces of tin and indium that would indicate that ITO@SiO₂ NPs disintegrated. We also evaluated the cytotoxicity of bare ITO and ITO@SiO₂ NPs at 0.25 wt% and found that neither variant decreased cell viability. Overall, these results indicate that an 0.25 wt% ITO@SiO₂ nanofluid would not pose a significant health risk to cells during laser lithotripsy.

Dedication

I want to dedicate this dissertation to my parents, Pedro Dominguez Martinez and Mayra Benitez Cedillo, my sister, Ibelizet Dominguez, my partner, Arjun Sridhar, and my dog, Nova. I also want to dedicate this work to my friends, Faisal Anees, Sam Abrams, Nathan Rayens, Cloie Dobias, Tori Kirby, Justin Sylvers, Kiko, John Levhan, Kate Klungtvedt, Margaret Brose, Caryn Wolter, Eric Mohr, Kenzie Boldt, Karsten Poulsen, Xu Han, Morgan Heckman. Without you all, this work would not have been possible.

Contents

| | |
|---|------|
| Abstract | iv |
| List of Tables..... | xii |
| List of Figures..... | xiii |
| Statement of Co-Authorship | xv |
| Acknowledgments..... | xvii |
| 1. Introduction | 1 |
| 1.1 Nanomaterial applications..... | 1 |
| 1.1.1 Size and surface area considerations..... | 2 |
| 1.2 Human exposure to nanomaterials | 2 |
| 1.2.1 Protein-nanomaterial interactions | 3 |
| 1.3 CNTs..... | 4 |
| 1.3.1 Inhalation of MWCNTs..... | 5 |
| 1.4 Kidney stone disease..... | 5 |
| 1.4.1 Kidney stone treatments | 6 |
| 1.5 Objectives and outline | 7 |
| 2. House dust mite extract forms a der p 2 corona on multi-walled carbon nanotubes: implications for allergic airway disease | 9 |
| 2.1 Introduction | 10 |
| 2.2 Materials and Methods..... | 13 |
| 2.2.1 Multi-walled carbon nanotube (MWCNT) characterization | 13 |
| 2.2.2 Rodent bronchoalveolar lavage fluid (BALF)..... | 14 |
| 2.2.3 Protein corona formation and concentration..... | 15 |

| | | |
|-------|--|----|
| 2.2.4 | Gel electrophoresis..... | 15 |
| 2.2.5 | Western blotting..... | 16 |
| 2.2.6 | Proteomic analysis..... | 17 |
| 2.3 | Results and Discussion..... | 18 |
| 2.3.1 | MWCNT characterization..... | 18 |
| 2.3.2 | House dust mite (HDM) extract forms a corona on MWCNTs | 19 |
| 2.3.3 | Concentration of the HDM corona (HDM-MWCNT) | 21 |
| 2.3.4 | Composition of HDM-MWCNT..... | 22 |
| 2.3.5 | Interaction of HDM-MWCNTs with lung fluid proteins..... | 25 |
| 2.3.6 | Interaction of HDM-MWCNTs with albumin | 28 |
| 2.4 | Conclusions | 31 |
| 2.5 | Supplementary material..... | 33 |
| 3. | Enzyme activity of cysteine and serine proteases adsorbed on to nanomaterials | 36 |
| 3.1 | Introduction | 36 |
| 3.2 | Materials and Methods..... | 38 |
| 3.2.1 | Nanoparticle (NP) preparation..... | 38 |
| 3.2.2 | Preparing protein mixtures and coronas..... | 38 |
| 3.2.3 | Protein concentration and proteolytic activity | 39 |
| 3.3 | Results and Discussion..... | 39 |
| 3.3.1 | Proteolytic activity of HDM and MWCNTs | 39 |
| 3.3.2 | Concentration of enzyme coronas on MWCNTs | 41 |
| 3.3.3 | Concentration of active enzymes on MWCNT coronas compared to free enzymes..... | 42 |

| | | |
|-------|--|----|
| 3.3.4 | Concentration of enzyme coronas on PS NPs..... | 44 |
| 3.3.5 | Concentration of active enzymes on PS enzyme coronas compared to free enzymes..... | 46 |
| 3.4 | Conclusions | 47 |
| 4. | Concentration of protein coronas on purified and functionalized MWCNTs as a function of initial protein concentration..... | 49 |
| 4.1 | Introduction | 49 |
| 4.2 | Materials and Methods..... | 51 |
| 4.2.1 | MWCNT characterization..... | 51 |
| 4.2.2 | Protein corona formation and concentration..... | 52 |
| 4.2.3 | Gel electrophoresis..... | 52 |
| 4.3 | Results and Discussion..... | 53 |
| 4.3.1 | Albumin adsorption on pristine, purified, and functionalized MWCNTs ... | 53 |
| 4.3.2 | HDM forms a corona on thermally and chemically purified MWCNTs..... | 56 |
| 4.3.3 | Composition of HDM coronas on pristine and purified MWCNTs..... | 57 |
| 4.4 | Conclusions..... | 58 |
| 5. | Indium tin oxide based nanofluid for laser lithotripsy treatment | 60 |
| 5.1 | Introduction | 61 |
| 5.2 | Materials and Methods..... | 62 |
| 5.2.1 | Inductively coupled plasma mass spectrometry (ICP-MS)..... | 62 |
| 5.2.2 | Cell culture..... | 63 |
| 5.2.3 | MTT assay | 63 |
| 5.3 | Results and Discussion..... | 64 |
| 5.3.1 | ITO@SiO ₂ nanoparticles are stable in solution..... | 64 |

| | | |
|-------|--|----|
| 5.3.2 | Indium and tin are not released from ITO@SiO ₂ nanoparticles following irradiation..... | 66 |
| 5.3.3 | Cells health is maintained following exposure to bare ITO nanoparticles ... | 68 |
| 5.3.4 | Cells remain healthy after interactions with ITO@SiO ₂ NPs | 69 |
| 5.4 | Conclusions | 70 |
| 6. | Conclusion..... | 72 |
| 6.1 | Summary Work | 72 |
| 6.2 | Future Work..... | 74 |
| 7. | References..... | 75 |
| 8. | Biography | 90 |

List of Tables

| | |
|--|----|
| Table 2-1. XPS analysis of MWCNTs with and without a HDM corona present..... | 19 |
| Table 2-2: Normalized abundance (% of total protein) of the top-10 proteins identified in HDM and the HDM corona formed on MWCNTs (HDM-MWCNT)..... | 25 |
| Table 2-3: Normalized abundance (% of total protein) of top-5 proteins identified in HDM-BSA-MWCNT and BSA-HDM-MWCNT coronas..... | 30 |
| Table 2-4: Spectral counts, reported as a percent of total signal, for the excised 15 kDa band of the HDM-MWCNT corona. Proteins with spectral counts >1% are listed. | 33 |
| Table 2-5: Spectral counts, reported as a percent of total signal, for the excised 12 kDa band of the HDM-MWCNT corona. Proteins with spectral counts >1% are listed. | 34 |
| Table 2-6: Normalized abundance (% of total protein) of the top-10 proteins identified in HDM and the HDM corona formed on MWCNTs (HDM-MWCNT)..... | 35 |
| Table 5-1: Indium and tin concentrations in each sample collected by separating the nanoparticles from the supernatant using centrifugation and a dialysis device. | 65 |
| Table 5-2: Concentration of indium and tin in supernatant and nanoparticles following irradiation. | 68 |

List of Figures

| | |
|---|----|
| Figure 2-1: Representative TEM image of MWCNTs. | 19 |
| Figure 2-2: Formation of a HDM corona on MWCNTs (HDM-MWCNTs). | 20 |
| Figure 2-3: Protein concentration of the HDM corona formed on MWCNTs. | 22 |
| Figure 2-4: Gel electrophoresis shows the proteins present in BALF and a corona formed from BALF (BALF-MWCNT)..... | 26 |
| Figure 2-5: Schematic showing the formation of sequential coronas formed from HDM and BALF incubated with MWCNTs. | 27 |
| Figure 2-6: Gel electrophoresis was used to compare the proteins present in coronas formed sequentially from HDM and BALF. | 28 |
| Figure 2-7: Gel electrophoresis was used to compare the proteins present in HDM alone, BSA alone, a HDM corona, a BSA corona, and sequential coronas..... | 29 |
| Figure 2-8: A Venn diagram shows the overlap of the top-5 proteins present in HDM extract alone, HDM-MWCNTs, HDM-BSA-MWCNTs. | 31 |
| Figure 2-9: Removal of unbound HDM, referred to as washing, consisted of centrifugation, removal of supernatant, and resuspension in PBS. | 33 |
| Figure 2-10: Western blotting using an antibody against der p 2 confirms the band visible at ~15 kDa is der p 2 (14 kDa)..... | 34 |
| Figure 3-1 Comparing the proteolytic activity of HDM, mixture of HDM and MWCNT, and an HDM corona on MWCNTs..... | 41 |
| Figure 3-2: Protein concentrations of enzyme coronas on MWCNTs..... | 42 |
| Figure 3-3: Comparing the proteolytic activity free enzymes and enzyme coronas on MWCNTs..... | 44 |
| Figure 3-4: Protein concentrations of enzyme coronas on PS compared to BSA coronas on PS. | 45 |
| Figure 3-5: Comparing the proteolytic activity free enzymes and enzyme coronas on PS nanoparticles..... | 47 |

| | |
|--|----|
| Figure 4-1: Schematic of the types of MWCNTs, including pristine, purified and functionalized varieties..... | 50 |
| Figure 4-2: Protein concentration of the HDM corona formed on pristine, purified, and functionalized MWCNTs..... | 55 |
| Figure 4-3: Protein concentration of the HDM corona formed on pristine, CP, and TP MWCNTs. | 57 |
| Figure 4-4: Gel electrophoresis used to compare the composition of HDM corona on pristine, CP, and TP MWCNTs..... | 58 |
| Figure 5-1: Measuring indium and tin in ITO@SiO ₂ supernatant..... | 65 |
| Figure 5-2: Schematic of collecting supernatant and ITO@SiO ₂ following irradiation..... | 66 |
| Figure 5-3: Viability of mIMCD-3 cells, measured with a MTT assay, after incubation with 0.25 wt% bare ITO. | 69 |
| Figure 5-4: Viability of mIMCD-3 cells, measured with a MTT assay, after incubation with 0.25 wt% ITO@SiO ₂ | 70 |

Statement of Co-Authorship

Chapters throughout this dissertation have been drawn from collaborative published studies. The co-authors contributions have been essential in producing manuscripts. I note the co-authors at the beginning of a chapter, and in this section, I will briefly detail author involvement.

In Chapter 2, my co-authors were with Samantha K. Holmes, Ryan D. Barton, Logan J. Tisch and Professors Robert M. Tighe, James C. Bonner and Christine K. Payne. I was responsible for charactering the nanomaterials and protein coronas, analysis of proteomic data, and data visualization. Samantha was responsible for verifying materials and methods, Ryan and Logan were responsible for analyzing protein coronas with a western blot. Dr. Tighe provided us with lung fluid from mice that was essential to our experiments and provided guidance on the research. Dr. Payne and Dr. Bonner provided essential context for the impact of the research and essential guidance on experiment design.

Chapter 5 was research accomplished by collaborating with Qingsong Fan, Junqin Chen, and Professors Pei Zhong, Po-Chun Hsu, and Christine K. Payne. I was responsible for characterizing samples, experimental design, analysis, data visualization, and conducting cell experiments. Qingsong was responsible for synthesizing the ITO nanoparticles. Junqin was responsible for laser exposure experiments. Faisal Anees was responsible for cytotoxicity protocols. Dr. Zhong, Dr. Hsu and Dr. Payne provided

essential context for the impact of the research and essential guidance on experiment design.

Acknowledgments

I would like to thank the Payne Lab for giving me the opportunity to learn and grow as a scientist and person. I am especially thankful to Christine Payne for guiding me through my PhD. To every one of my current and past lab mates, your support and friendship is something I will always be immensely grateful for. The Payne Lab was a wonderful space I was glad to be a part of.

I want to thank my committee, Dr. James Bonner, Dr. Pei Zhong, and Dr. Walters for providing constructive feedback and guidance throughout our time working together.

All the friends I've made in Durham will always hold a place in my heart. Thank you to everyone that I've shared laughter, hikes, dinners, and movie nights. Sharing these moments helped me remember to enjoy life amid stressful times.

None of this would have been possible without everyone mentioned. Thank you everyone for your support.

1. Introduction

Nanomaterials are materials that have at least one dimension or is reduced in composition to a nanoscale range.¹ According to the nanomaterial dimensionality, nanomaterials can be classified into four groups. Nanoparticles, fullerenes, and quantum dots are classified as zero-dimensional nanomaterials. One-dimensional nanomaterials have one dimension outside of the nanometer scale. This includes nanowires, nanotubes, and nanofibers. Two-dimensional nanomaterials have two dimensions outside of the nanometer scale, which includes nanofilms, nanosheets, and nanolayers. Three dimensional or bulk materials include core shells, nanowire arrays, and nanotube arrays. These nanomaterials are not in the nanoscale in any dimension.²⁻⁴ Due to diversity of sizes, surface effects, and quantum tunnel effects, nanomaterials have captured the attention of the researchers.⁵

1.1 *Nanomaterial applications*

The global market for nanomaterials was over 1.6 million tons in 2020, and it is expected to double to 3.5 million metric tons by 2031.⁶ Further analysis of this projection allows nanomaterial consumption to be classified by application. These applications include, but are not limited to, fuel cells, energy storage, lubricants, textiles and adsorbent applications.^{6,7} Physical and chemical properties, such as high surface to volume ratio and size, are the factors considered by the end user.⁸

1.1.1 Size and surface area considerations

The size of a nanoparticles (NPs) is correlated to the surface area, such that as the NP size decreases, the surface area increases exponentially.⁹ This change in dimensionality impacts the reactivity of the NPs. For example, small NPs can more readily adsorb into plant and animal tissues. In some applications, such as in drug delivery, being able to readily adsorb into biological tissues can be beneficial. However, in the instances where a nanomaterial could pose a toxicity to living organisms, the ability for small NPs to penetrate barriers is a risk of high concern. Some examples of nanomaterials that present possible risks include manganese dioxide (MnO₂), titanium dioxide (TiO₂) and carbon-based nanomaterials. These nanoparticles pose a risk to the brain through potential interactions with the nasal epithelium olfactory neurons.¹⁰⁻¹² Particles with a size less than 100 nm can cross cell membrane and enter the cells. Larger particles with size range from 200-500 nm can also enter cells, but at a lower risk.^{9,10,13,14}

1.2 Human exposure to nanomaterials

As nanomaterial usage increases, we need to better understand the health effects of human exposure to these unique nanomaterials.¹⁵ Cosmetic products, such as sunblock, can often contain zinc oxide (ZnO) as an ultraviolet inorganic filter for UVB (290-320 nm) and UVA (320-400 nm). Another common pathway for human exposure to nanomaterials is in a manufacturing setting. Nanomaterials are crucial to the development of technology and electronics.¹¹ For example, silicon and thin-film transistors offer high performance but are limited to miniaturization.¹⁶ Use of

nanomaterials like carbon nanotubes, graphene, and molybdenum disulfide would allow for transistors to be scaled down 10 nm, without sacrificing performance.¹⁷ Although nanomaterials provide opportunities for technological advancements. Exposure to these nanomaterial are a concern for the people manufacturing these devices.¹⁸⁻²³

Inhalation is an exposure pathway of particular concern, as nanomaterials can be easily aerosolized.²⁴ Previous studies have found that the inhalation of nanomaterials results in inflammatory reaction in the lung and potential effects to other organs.²⁵ Nanomaterial effects on the respiratory tract are depend on the material physicochemical characteristics and the biological environment. Nanomaterials between 10-50 nm end up in alveoli, while those smaller than 10 nm and larger than 50 nm can become deposited in higher regions of the lung.²⁶ Additionally, the toxicity of nanofibers, such as carbon nanotubes (CNTs), has been extensively studied.²⁷⁻³² Inhalation of high concentrations single-walled CNTs (SWCNTs) and multi-walled CNTs (MWCNTs) induced neutrophil inflammation and granulomatous formations in the lung.^{33,34} The increased surface area and aggregation of CNTs are properties that increase the rate of neutrophils in the lung.³⁴

1.2.1 Protein-nanomaterial interactions

Biological interactions with nanomaterials result in the interaction of proteins present in a biological system with the nanomaterials. This interaction is the foundation of nanoparticle bioreactivity.³⁵ In a physiological environment, protein adsorb onto the

surface of a nanomaterials to form a protein 'corona'.³⁶ Protein coronas alter the biological response to nanomaterials. Therefore, understanding the composition and the factors that affect the protein corona are essential in understanding the biological effects of nanomaterials.

1.3 CNTs

Carbon is made up of six electrons in the 1 s^2 , 2 s^2 , and 2 p^2 . This element can also hybridize in sp , sp^2 , or sp^3 forms. Materials such as graphene, fullerenes, and CNTs are very constant sp^2 bonded materials. Graphene is composed of densely organized carbon atoms in a sp^2 -bonded atomic-scale honeycomb (hexagonal) pattern. This pattern is the blueprint for fullerenes and CNTs. A CNT is a result of rolled up sheet of graphene. Arc discharge, laser ablation, and chemical vapor deposition are the processes used to synthesize CNTs.³⁷ SWCNTs are made up of a single layer of graphene.³⁸

In contrast, MWCNTs are made up of three or more concentrically organized sheets of graphene. The distance between each wall is approximately 0.340 nm.³⁹ Multi-walled carbon nanotubes (MWCNT) are used for applications, such as electronics, gene delivery, coatings, and material composites.⁴⁰⁻⁴² The stability, tensile strength, electric conductivity, and thermal resistance have made MWCNTs an appealing material to agriculture, energy, and automotive industries.^{43,44}

1.3.1 Inhalation of MWCNTs

As indicated in section 1.2, human exposure is a major concern as the use of nanomaterials increases. The physiological responses to the inhalation of MWCNTs have been previously studied. It was found that MWCNTs caused lung inflammation and fibrosis in rodents.⁴⁵ When MWCNTs are well dry or dispersed in a surfactant solution, macrophages are more available for macrophage uptake, as opposed to MWCNTs aggregates that pose a challenge for the immune system.⁴⁶ Therefore, changes in MWCNTs surface treatments and functionalization can alter the physiochemical response.⁴⁶ Beyond analyzing the cellular responses to MWCNTs, lung protein interactions with MWCNTs need to be investigated. When MWCNTs are inhaled, lung fluid proteins will adsorb onto the surface of the MWCNTs. These lung fluid proteins form a protein corona that influence the biological response to MWCNTs.^{47,48}

1.4 Kidney stone disease

Kidney stone disease rates have been consistently increasing over the past 50 years due to changes lifestyle, dietary habits and global warming. Kidney stones are mineral deposits in the renal calyces and pelvis. These minerals can either be found free or attached to the renal papillae. Approximately 80% of kidney stones are made up of calcium oxalate mixed with calcium phosphate.⁴⁹

1.4.1 Kidney stone treatments

The size and location of kidney stones can vary from case to case. In an attempt to provide treatment for the variety of cases, physicians chose between three types of medical procedures. Shockwave lithotripsy is a non-invasive procedure currently available and allows for the fragmentation of <1 cm stones when located in the lower pole of the kidney and stones over <2 cm when located in the middle and upper poles.⁴⁹⁻

⁵¹ During this procedure high energy acoustic waves, produced by electrohydraulic, electromagnetic or other types of energy sources, are used to fragment the stones.⁵²

Ureteroscopic fragmentation and retrieval is another method commonly used for 1-1.5 cm stones in the lower pole and stones <2 cm when located in the middle and upper poles.⁴⁹ Laser lithotripsy is a type of ureteroscopic fragmentation, in which an endoscope is inserted through the urethra and guided to the affected kidney.⁵³ A laser is also inserted, which will produce energy pulses to fragment the stones. The holmium yttrium-aluminum-garnet (Ho:YAG) laser is preferred due to the rapid absorption in water and minimal tissue penetration.⁵⁴⁻⁵⁶ Finally, percutaneous nephrolithotomy is considered for stones >2 cm in the middle and upper poles.⁵⁷ This is the most invasive type of treatment because it requires an endoscope to be percutaneously passed through skin, muscle and perirenal fat, in order to reach the kidney.⁴⁹ Once access is achieved the stones are fragmented or removed.⁵⁷

1.5 Objectives and outline

Chapter 2 showcases our work toward understand how MWCNTs interact with the protein environment of the lung and inhaled allergens. House dust mite (HDM) allergens, known to trigger allergic airway diseases, particularly asthma, are of particular interest. The protein coronas formed by the adsorption of these biomolecules on to MWCNTs were characterized for individual proteins and proteins in combination. Gel electrophoresis, western blots, and proteomics were used to determine the resulting protein corona. We found that der p 2, a protein associated with human allergic responses to HDM, dominates the composition of coronas following subsequent exposures to lung fluid proteins. This chapter is adapted from my first author publication in *Environmental Science Nano* coauthored with Samantha K. Holmes, Ryan D. Barton, Logan J. Tisch and Professors Robert M. Tighe, James C. Bonner and Christine Payne.

Chapter 3 further explores the implications of HDM and MWCNT interactions. We evaluated the enzyme activity of HDM allergens allows us to determine whether HDM and MWCNTs interactions could exacerbate allergic airway disease. Trypsin and papain enzyme coronas on MWCNTs and polystyrene nanoparticles were used as comparisons. Results revealed no enhancement in enzyme activity on either material.

Chapter 4 characterizes albumin adsorption on pristine, purified, and functionalized MWCNTs exhibited distinct adsorption profiles depending on the surface modification. Thermally purified MWCNTs with and without the addition of carboxyl

groups showed no significant changes in protein adsorption as albumin concentration increased.

Chapter 5 explores how nanomaterials also have potential to advance medical technologies. We characterized indium tin oxide nanoparticles coated with silica dioxide (ITO@SiO₂ nanofluid) to reduce thermal damage during kidney stone laser lithotripsy. Stability tests showed no evidence of nanoparticle disintegration in solution or under extreme laser exposure. Cytotoxicity testing at 0.25 wt% indicated low risks to cell viability. These findings suggest MWCNT interactions with lung proteins and allergens are complex, and that ITO@SiO₂ nanofluid is promising for lithotripsy, demonstrating the versatile applications and relative safety of nanomaterials. This chapter highlights research conducted in collaboration with Qingsong Fan, Junqin Chen, and Professors Pei Zhong, Po-Chun Hsu, and Christine K. Payne

2. House dust mite extract forms a der p 2 corona on multi-walled carbon nanotubes: implications for allergic airway disease¹

MWCNTs are used in materials for the construction, automotive, and aerospace industries. Workers and consumers are exposed to these materials *via* inhalation. Existing recommended exposure limits are based on MWCNT exposures that do not take into account more realistic co-exposures. Our goal was to understand how a common allergen, house dust mite extract, interacts with pristine MWCNTs and lung fluid proteins. We used gel electrophoresis, western blotting, and proteomics to characterize the composition of the allergen corona formed from house dust mite extract on the surface of MWCNTs. We found that the corona is dominated by der p 2, a protein associated with human allergic responses to house dust mites. Der p 2 remains adsorbed on the surface of the MWCNTs following subsequent exposures to lung fluid proteins. The high concentration of der p 2, localized on surface of MWCNTs, has important implications for house dust mite-induced allergies and asthma. This research provides a detailed characterization of the complex house dust mite-lung fluid protein coronas for future cellular and *in vivo* studies. These studies will help to address the molecular and biochemical mechanisms underlying the exacerbation of allergic lung disease by nanomaterials.

¹ This chapter comes from my published first-author paper (Dominguez et al. 2024). Co-authors on this paper include Samantha K. Holmes, Ryan D. Bartone, Logan J. Tisch, and Professors Robert M. Tighe, James C. Bonner, and Christine Payne.

2.1 Introduction

MWCNTs are essential components of electronics, plastics, sensors, and coatings with applications in the construction, automotive, and aerospace industries.^{58,59} Given this wide range of applications, it is important to understand the effects that MWCNTs may have on both workers in the manufacturing setting and consumers who are exposed to these materials following environmental release. Inhalation is of specific concern as this is the primary route of exposure.⁶⁰⁻⁶³ The pulmonary toxicity of MWCNTs in rodents is well-demonstrated and known to be dependent on the physicochemical characteristics of the MWCNTs.^{45,64-70} For example, rigid, rod-like MWCNTs are more toxic than flexible, tangled, MWCNTs.⁷¹ The National Institute for Occupational Safety and Health (NIOSH) provides an overview of the occupational hazards associated with these materials and recommended exposure limits.⁷² These recommended exposure limits are based solely on MWCNT exposure that do not take into account more realistic co-exposures. For example, allergic lung disease induced by common allergens, such as those from house dust mites (HDM; *Dermatophagoides pteronyssinus*), is exacerbated by MWCNT inhalation exposure in mice.⁷³ These findings suggest that the current exposure limits to MWCNTs should take into account co-exposures. In addition, the mechanistic details underlying the observed toxicity of these nanomaterial-allergen co-exposures are lacking, especially regarding the initial steps of inhalation and the relationship of material properties to physiological and pathological outcomes.^{74,75}

Previous work has shown that blood serum proteins and cell lysates adsorb on the surface of MWCNTs forming a protein corona.⁷⁶⁻⁷⁹ The protein corona, rather than the bare nanomaterial, determines the subsequent biological events including cellular internalization and immune response.^{47,80-85} Our research focuses on the formation of an allergen corona as MWCNTs interact with allergens in the environment, followed by the interaction of these allergen-MWCNTs with lung fluid obtained from mice. The interaction of titanium dioxide and polystyrene nanoparticles with bronchoalveolar lavage fluid (BALF) has been characterized previously.^{86,87} For the titanium dioxide nanoparticles, a BALF corona led to increased expression of pro-inflammatory cytokines in macrophages.⁸⁷ To the best of our knowledge, our work described below is the first to address a combined allergen and lung fluid corona.

We examine one common allergen, HDM extract. Allergies to HDM are estimated to affect 1-2% of the global population.⁸⁸⁻⁹⁰ Eighty-five percent of asthmatics are allergic to HDM.⁹¹ HDM extract is a multi-component allergen consisting of a mixture of proteins from mites, nymphs, fecal matter, and eggs.⁹²⁻⁹⁵ Of specific interest are two proteins, der p 1 and der p 2.⁹³ The majority (~80%) of people with HDM allergies are sensitive to der p 1 and der p 2.⁹⁶ Sera samples from allergic subjects showed that 50% of IgE binding was directed at these two proteins.⁹⁷ Der p 1 is a cysteine protease.⁹⁸⁻¹⁰¹ Der p 2 is a myeloid differentiation factor-2-related lipid recognition domain lipid-binding family protein,¹⁰² which is found in the digestive track and feces of HDM.¹⁰³ Previous work has suggested that a HDM corona on MWCNTs

could be a factor in the exacerbated allergic airway disease observed in mice.¹⁰⁴ *In vitro* experiments examined gold nanoparticles (50 nm) conjugated to der p 1.¹⁰⁵ Proteolytic assays showed that the der p 1-gold nanoparticle conjugates had increased proteolytic activity compared to der p 1,¹⁰⁵ suggesting that allergen coronas may amplify allergic responses. This is supported by *in vivo* experiments showing that mice co-exposed to MWCNTs and HDM extract displayed increased allergic lung inflammation that was not observed with MWCNTs or low doses of HDM extract alone.⁷³

In terms of human exposures, MWCNTs could encounter HDM in both manufacturing and consumer settings. HDM are ubiquitous in the indoor environment: they thrive in upholstered furniture, carpets, bedding, and dust. Previous work has found that MWCNTs were present in the office areas adjacent to production facilities.¹⁰⁶ In these office areas, MWCNTs would certainly come into contact with HDM. This study did not measure HDM in the MWCNT production facility, but it is likely that such facilities also contain some HDM, especially in production areas that may contain dust. It is also possible that MWCNTs and HDM will come into contact during the life cycle of the nanomaterial, where there is release of MWCNTs from a matrix or during recycling.¹⁰⁷ For example, the future use of MWCNTs in textiles would result in consumer exposure within homes that contain HDM.

Our approach, described below, was to characterize the protein corona formed on MWCNTs incubated with HDM extract, both alone and in combination with BALF. We focus on a single type of MWCNT (NC7000), which is the parent nanomaterial that

can be further chemically or thermally purified and functionalized.⁴⁵ We use gel electrophoresis, western blotting, and proteomics to characterize the composition of the protein corona. We found that HDM extract forms a corona on the surface of MWCNTs and that this corona is dominated by der p 2. Der p 2 remains adsorbed on the MWCNTs following subsequent exposures to BALF or albumin, the main protein present in BALF. The high concentration of der p 2, localized on surface of MWCNTs, has important implications for HDM-induced allergies and asthma. This research will help to address the molecular and biochemical mechanisms underlying the exacerbation of allergic lung disease by nanomaterials and provides a detailed characterization of these complex protein coronas for future cellular and *in vivo* studies.

2.2 Materials and Methods

2.2.1 Multi-walled carbon nanotube (MWCNT) characterization

MWCNTs (NC7000, Nanocyl, Sambreville, Belgium) were used for all experiments. Stock solutions of MWCNTs were prepared by suspending dry MWCNTs (10 mg mL⁻¹) in 1× phosphate buffered saline (PBS; 21300025, Thermo Fisher, Waltham, MA). Solutions were sonicated for five minutes with a cup horn sonicator (40% amplitude; Q500 Sonicator, Q Sonica, Newtown, CT) to help suspend the MWCNTs.

Transmission electron microscopy (TEM; Talos F200X, Thermo Fisher) was used to quantify the diameter of the MWCNTs. A MWCNT solution (100 µg mL⁻¹ in PBS) was drop-cast onto carbon coated copper grids (FCF200-Cu, Electron Microscopy Sciences, Hatfield, PA). Images were collected with 50k× magnification at 200 kV. ImageJ was

used for image analysis.¹⁰⁸ X-ray photoelectron spectroscopy (XPS; Kratos Analytical Axis Ultra, Shimadzu Corporation, Kyoto, Japan) at the Shared Materials Instrumentation Facility at Duke University was used to measure the elemental composition of the MWCNTs.

2.2.2 Rodent bronchoalveolar lavage fluid (BALF)

Our procedure for obtaining BALF has been described previously.⁸⁷ All procedures were approved by the Duke University Institutional Animal Care and Use Committee (IACUC) and were performed under an IACUC approved animal protocol (A053-21-03). All animal experiments were conducted in accordance with the American Association for the Accreditation of Laboratory Animal Care guidelines. In brief, C57BL/6 male mice (8–10 weeks) were purchased from Jackson Laboratories (Bar Harbor, ME). Bronchoalveolar lavages were performed following a published protocol.¹⁰⁰ Prior to lavage, mice were deeply anesthetized with an intraperitoneal injection of ketamine (100 mg kg⁻¹), xylazine (100 mg kg⁻¹), and saline (0.9%), dosed by weight (350–500 µL). The chest and trachea were dissected to expose the lungs and trachea. Tubing (PE-60, #9565S30, Thomas Scientific, Swedesboro, NJ) was inserted into the trachea and attached to a 12-inch infusion set (#SV-25BLK, Terumo, Tokyo, Japan) connected to a 10 mL syringe held on a ring stand. Lungs were passively filled to 20 cm H₂O with PBS to reach total lung capacity. The BALF was then passively drained and placed on ice for further processing. BALF used for protein corona formation was pooled from 10–20 mice to reduce mouse-to-mouse variation.

2.2.3 Protein corona formation and concentration

Protein coronas were formed by incubating MWCNTs with proteins for 30 minutes at room temperature (RT) on an orbital shaker (700 rpm, 88882006, Digital Microplate Shaker, Thermo Fisher). Proteins used included HDM (*Dermatophagoides pteronyssinus*, XPB91D3A2.5, Lot 414145, Stallergenes Greer, Lenoir, NC), bovine serum albumin (BSA; A2153-50G, Sigma-Aldrich, St. Louis, MO), and BALF. To remove unbound protein, samples were washed three times by centrifugation (15–30 minutes, 4 °C, 14 000 rpm) and resuspension in PBS. Removal of unbound and weakly bound proteins results in a “hard” corona. To create sequential coronas, the corona formation procedure was repeated using a second protein. Protein concentrations were measured with a colorimetric assay (Pierce 660 nm Protein Assay, referred to as a 660 nm assay, 2260, Thermo Fisher Scientific) and quantified with a plate reader (SpectraMax iD3, Molecular Devices, San Jose, CA).

2.2.4 Gel electrophoresis

The compositions of the protein coronas were visualized using gel electrophoresis. Protein–MWCNT complexes were resuspended in Laemmli SDS-sample buffer (4×, reducing, BP-110R, Boston BioProducts, Milford, MA). Proteins were denatured by boiling samples at 95 °C for 5 minutes before loading into a tris-glycine sodium dodecyl sulfate (SDS) precast polyacrylamide gel (4561096, Bio-Rad Laboratories, Hercules, California). A 10–250 kDa molecular weight marker (Precision Plus Protein Dual Color Standards, 1610374, Bio-Rad) was included in the gel. A voltage

of 230 V was applied for 30 minutes. The gel was rinsed by microwaving in deionized water three times (1 minute heat, 1 minute rocking at RT, water replaced). The gel was then stained (SimplyBlue Safe Stain, LC6060, Thermo Fisher) by microwaving for 45 seconds and rocking for 5 minutes at RT. Deionized water was used to destain the gel (rocking overnight, RT) before imaging (PhotoDoc-It; Analytik Jena, Jena, Germany).

2.2.5 Western blotting

Gels for western blotting were transferred to a 0.2 mm PVDF membrane (1704156, Bio-Rad Laboratories) using the Trans-Blot Turbo Transfer System (1704150, Bio-Rad Laboratories) and run at 2.5 A for 7 min. Membranes were blocked (5% dry milk in tris-buffered saline with 0.1% Tween buffer) for 1 hour and then incubated overnight in a 1 : 1000 dilution of a polyclonal anti-der p 2 (AA 18-146) antibody (ABIN7141165, Antibodies-online Inc., Limerick, PA). Following primary antibody incubation, the membranes were washed and incubated in 1 : 2000 dilution with horseradish peroxidase-conjugated secondary anti-rabbit antibody (#7074, Cell Signaling Technology, Danvers, MA). Enhanced chemiluminescence (ECL) Prime Western Blotting Detection Reagent (Cytiva, Marlborough, MA) was used to for HRP-induced chemiluminescence, and the resulting signals were imaged using an Amersham Imager 680 (GE Life Sciences, Marlborough, MA).

2.2.6 Proteomic analysis

Proteins were removed from the MWCNT surface by incubation with 5% SDS buffer for 5 minutes at 95 °C. A 660 nm assay was used to determine protein concentrations prior to submission for proteomic analysis. Individual bands for proteomic analysis were excised from the polyacrylamide gels and submitted without further processing.

The compositions of the protein coronas on MWCNTs were determined using liquid chromatography with tandem mass spectrometry (LC-MS/MS). Proteomic analysis was conducted by the Proteomics and Metabolomics Core Facility, part of the Duke Center for Genomics and Computational Biology. A UPLC column (75 μm \times 250 mm, nanoAcquity, Waters Corporation; 400 nL min⁻¹) with a 60 minute elution time was used for NanoFlow liquid chromatography with an acetonitrile gradient (5–40%) and 0.1% formic acid. In-line tandem mass spectrometry was used to analyze peptide fragments (Orbitrap Fusion Lumos, Thermo Fisher). We analyzed the LC-MS/MS data using MaxQuant (v2.1.0, Max Planck Institute, Munich, Germany).^{109,110} The raw LC-MS/MS spectra were searched using the integrated Andromeda search engine against the Swiss-Prot *Dermatophagoides pteronyssinus* (European house dust mite; #6956) and *Bos taurus* (bovine; #9913) canonical protein databases from UniProt, accessed on June 5th, 2023. A custom contaminants file was used while searching, which contained a relevant subset of the Common Repository of Adventitious Proteins (cRAP) database.¹¹¹ For protein and peptide quantification and identification, default MaxQuant parameters

were used including a 0.01 false discovery rate, a minimum peptide length of 7 amino acids, a maximum peptide length of 25 amino acids, oxidation and acetyl groups as variable modifications, and carbamidomethyl as a fixed modification.

Perseus (v2.0.3.1, Max Planck Institute) was used to analyze and filter proteomic data.¹¹² Proteins were excluded if they were contaminants, quality control standards, or were not observed in at least 2 samples. A quantitative internal standard was not used for these experiments. The intensities of all proteins identified within a sample were summed to obtain the relative abundance of each protein within each sample triplicate. Averages and standard deviations were calculated from the abundances of the sample triplicates. The mass spectrometry proteomics data have been deposited to the ProteomeXchange Consortium *via* the Proteomics Identification Database (PRIDE) partner repository with the dataset identifier PXD047039.

2.3 Results and Discussion

2.3.1 MWCNT characterization

The diameter of the MWCNTs was measured from TEM images (Fig. 1). Dynamic light scattering is not suitable for these filamentous, non-spherical samples. The MWCNTs have an average diameter of 11.9 ± 0.6 nm ($n = 6$), in good agreement with previous TEM experiments showing a diameter of 12 nm.^{45,113} XPS analysis of MWCNTs revealed a composition of 98.33% carbon, 1.49% oxygen, and 0.18% aluminum (Table 1). A previous analysis of these MWCNTs with XPS found similar levels of carbon (97.8%)

and oxygen (1.4%).⁴⁵ Trace amounts of aluminum are attributed to the synthesis process, in which metal oxides are present during catalytic chemical vapor deposition.^{60,114–117}

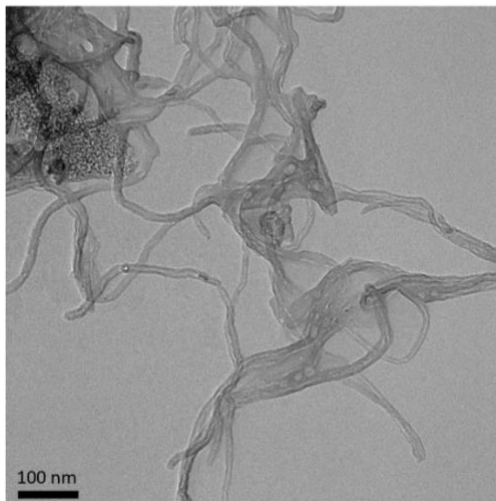


Figure 2-1: Representative TEM image of MWCNTs.

Table 2-1. XPS analysis of MWCNTs with and without a HDM corona present.

| Sample | Elemental Analysis (%) | | | | |
|-----------|------------------------|-------|------|------|------|
| | C | O | Al | N | Na |
| MWCNT | 98.33 | 1.49 | 0.18 | - | - |
| HDM-MWCNT | 72.01 | 22.08 | 0.20 | 2.93 | 2.31 |

2.3.2 House dust mite (HDM) extract forms a corona on MWCNTs

We first characterized the corona that forms on MWCNTs following incubation with HDM extract using gel electrophoresis (Fig. 2). MWCNTs (1 mg mL^{-1}) were incubated with HDM (1 mg mL^{-1}) in PBS (30 minutes, RT) then washed to remove unbound protein, as described in Materials and methods (Fig. 2A and S1†). XPS shows that MWCNTs with a HDM corona (HDM-MWCNT) are similar in composition to the pristine MWCNTs, but with an increase in the percentage of oxygen (22.08%) and the

addition of nitrogen (2.93%) and sodium (2.31%) (Table 1), likely reflecting the presence of protein and PBS used to form the protein corona. Gel electrophoresis was used to separate and identify the specific proteins that comprise the HDM-MWCNT corona (Fig. 2B). In comparison to HDM alone, the corona formed on MWCNTs (HDM-MWCNT) shows an increase in the band at ~15 kDa and the appearance of a ~12 kDa band. These bands were excised and submitted for proteomics. Based on spectral counts, they were identified to be der p 2 (14 kDa) and der p 30 (12 kDa) (Tables S1 and S2[†]). In addition, western blotting confirms the ~15 kDa band is der p 2 (Fig. S2[†]).

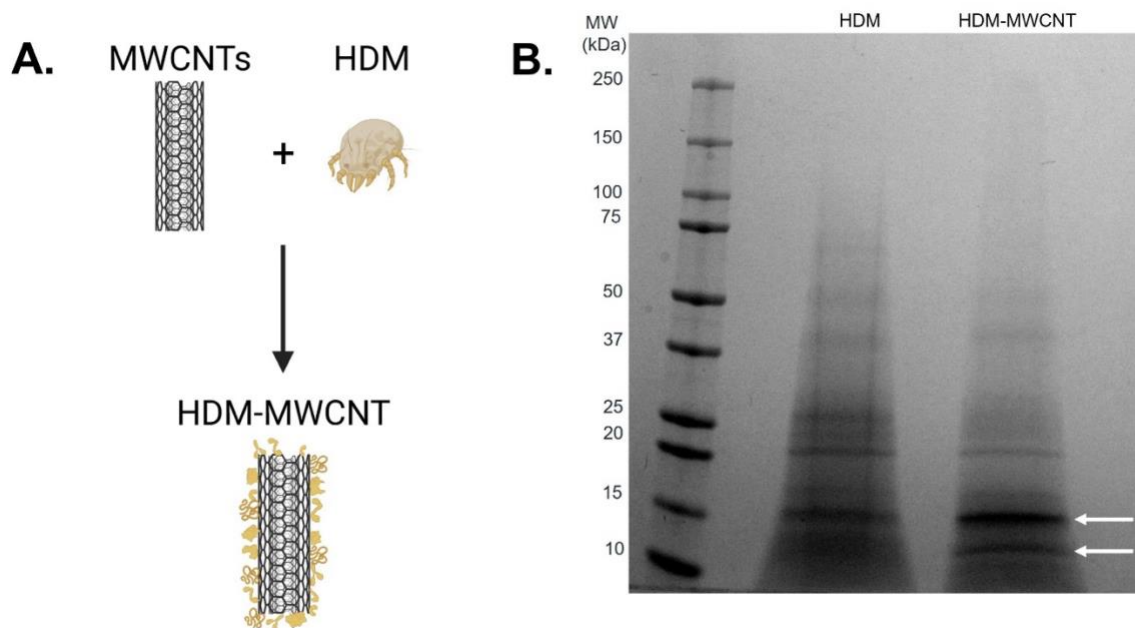


Figure 2-2: Formation of a HDM corona on MWCNTs (HDM-MWCNTs). A. Schematic showing the formation of a HDM corona. B. Gel electrophoresis shows the

proteins present in HDM compared to the HDM corona formed on MWCNTs. Bands at ~15 kDa and ~12 kDa are highlighted with arrows.

2.3.3 Concentration of the HDM corona (HDM-MWCNT)

The concentration of HDM proteins that adsorb on the surface of MWCNTs was quantified using a 660 nm protein assay (Fig. 3). MWCNTs (1 mg mL^{-1}) were incubated with increasing concentrations of HDM ($0.1\text{--}2.0 \text{ mg mL}^{-1}$). Samples at lower incubation concentrations (0.1 mg mL^{-1} and 0.25 mg mL^{-1} HDM) were pooled ($\times 3$) for measurement to provide sufficient protein for the assay. The resulting concentration of protein adsorbed on the MWCNTs increases from 0.1 mg mL^{-1} to 0.5 mg mL^{-1} and then remains constant with increasing HDM. The maximum concentration of protein in the corona is $7.69 \pm 0.80 \text{ } \mu\text{g mg}^{-1}$ MWCNT, calculated as the average of the samples formed with $0.5\text{--}2.0 \text{ mg mL}^{-1}$ of HDM. This increasing corona concentration as a function of increasing incubation protein concentration is in agreement with other corona studies. Similar assays with polystyrene and silica nanoparticles have shown that increasing the incubation protein concentrations leads to increasing corona concentrations,¹¹⁸⁻¹²¹ with rare exceptions.¹¹⁸ However, the maximum corona concentration is low compared to previous studies. For example, titanium nanoparticles incubated with fetal bovine serum form a corona of $50 \text{ } \mu\text{g protein/mg}$ of titanium dioxide nanoparticles.⁸⁷ It is possible that HDM, which is a mixture of mites, nymphs, fecal matter, and eggs,⁹² results in maximum corona formation at relatively low corona concentrations values. In

comparison, much of the previous work has focused on human plasma or bovine serum relevant to cell culture and biomedical applications.

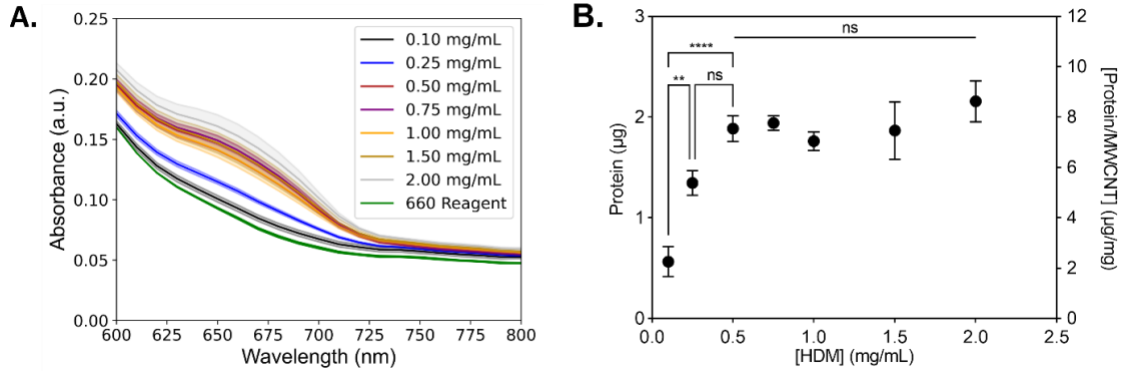


Figure 2-3: Protein concentration of the HDM corona formed on MWCNTs. A. MWCNTs were incubated with increasing concentrations of HDM (0.5–2 mg mL⁻¹). The concentration of the resulting corona was measured with a colorimetric protein assay (660 nm assay; $n = 3$ distinct samples). Solid lines show the mean and shading shows the standard deviation. Low concentration samples (0.1 mg mL⁻¹ and 0.25 mg mL⁻¹) were pooled for measurement ($\times 3$). **B.** Protein concentration of the resulting corona. The low concentration samples (0.1 mg mL⁻¹ and 0.25 mg mL⁻¹) are plotted at their $n = 1$ value. Significance was calculated using an ANOVA with a *post hoc* Tukey test. ** $p < 0.01$, **** $p < 0.0001$, ns = not significant.

2.3.4 Composition of HDM-MWCNT

Although gel electrophoresis provides a visualization of the corona proteins (Fig. 2B), proteomics provides a more detailed description of the composition of the protein corona (Table 2). Proteomic analysis is shown as the normalized abundance for HDM alone and the HDM corona (HDM–MWCNT). 79 proteins were identified in HDM and 46 proteins were identified in the HDM–MWCNT coronas. The top-10 of each sample ($n = 3$) are listed. Previous proteomics studies of HDM alone have identified a complex mixture of proteins.^{94,95} Der p 30, der p 2, der p 36, der p 1, and der p 10 have all

previously been identified as highly abundant proteins in mite bodies or extracts.^{94,95} Der p 27, observed in *D. farinae*,⁹⁵ was not observed at high abundance in *D. pteronyssinus* previously.

We compare the protein abundance in HDM to the corona formed on MWCNTs. For example, der p 30 is the most highly abundant protein ($29.3 \pm 13.3\%$) in the HDM extract, but it was observed at very low levels in the corona ($1.00 \pm 1.51\%$). Der p 2 is much less abundant in HDM ($12.7 \pm 9.01\%$), but the most abundant allergen in the HDM corona ($49.6 \pm 15.2\%$). Der p 36 was the second most highly abundant protein in the corona ($14.3 \pm 0.98\%$), although not highly abundant in HDM extract ($3.73 \pm 3.14\%$), showing that it is enriched in the corona. Der p 1, which, along with der p 2, is a major human allergen,^{93,97} was observed at low abundance in this lot of HDM ($1.79 \pm 0.54\%$) and the corona ($0.17 \pm 0.17\%$). The same analysis, using a different lot of HDM, also showed der p 2 was the most abundant protein in the corona ($51.6 \pm 15.6\%$), although there were lot-to-lot variations in the HDM and resulting corona (Table S3†). This lot-to-lot variation in HDM is expected based on previous work.¹²²

A direct comparison of gel electrophoresis and proteomics is complicated by overlapping molecular weights of proteins and different levels of protein staining. For example, based on proteomics data, der p 30 is highly abundant in HDM extract ($29.3 \pm 13.3\%$), but difficult to resolve in the gel (Fig. 2B). Gel electrophoresis of the corona results in fewer fragments and a cleaner gel resulting in a visible band at 12 kDa, although the abundance of der p 30 is relatively low ($1.00 \pm 1.51\%$) by proteomics.

Proteomics of the excised bands at 12 kDa and 15 kDa confirms the presence of der p 30 in the corona and the enrichment of der p 2 (Fig. 2B and Tables S1 and S2†).

Overall, the comparison between HDM and HDM-MWCNTs shows that der p 2 is highly concentrated on the surface of MWCNTs, which may be important for allergic airway disease. Der p 1, which is the other major human allergen, was identified in the protein corona at very low abundance.^{93,96,97}

Table 2-2: Normalized abundance (% of total protein) of the top-10 proteins identified in HDM and the HDM corona formed on MWCNTs (HDM-MWCNT). Proteins are ordered by abundance in HDM. Proteins present in a sample, but not in the top-10, are shown in italics. Proteins with normalized abundance < 0.1% are not shown. The most abundant protein in each sample is bolded. Mean and standard deviation are reported (n=3). For allergens, the biochemical name from the WHO/IUIS database is provided in parentheses.

| Protein | MW (kDa) | HDM (%) | HDM-MWCNT (%) |
|---|----------|--------------------|--------------------|
| Der p 30 (ferritin) | 12 | 29.3 ± 13.3 | 1.00 ± 1.51 |
| Uncharacterized protein LOC113797715 | 191 | 18.1 ± 6.71 | 0.39 ± 0.29 |
| Der p 2 (NPC2 family) | 14 | 12.7 ± 9.01 | 49.6 ± 15.2 |
| Fatty acid-binding protein-like | 15 | 5.97 ± 4.61 | 7.49 ± 9.79 |
| Der p 36 (C2 domain containing protein) | 25 | 3.73 ± 3.14 | 14.3 ± 0.98 |
| Der f 27 (serpin) | 47 | 2.03 ± 0.85 | 1.16 ± 1.34 |
| Der p 1 (cysteine protease) | 24 | 1.79 ± 0.54 | 0.17 ± 0.17 |
| Der p 10 (tropomyosin) | 33 | 1.69 ± 1.53 | 3.90 ± 3.89 |
| Peptidase 1-like | 39 | 1.62 ± 0.31 | - |
| Fructose-bisphosphate aldolase | 39 | 1.44 ± 2.35 | - |
| Nucleoside diphosphate kinase | 18 | 0.91 ± 0.68 | 4.03 ± 0.66 |
| Der p 7 (bactericidal permeability increasing-like) | 24 | 0.12 ± 0.067 | 3.09 ± 1.09 |
| Der f 22 (Group 2-like) | 18 | - | 2.46 ± 3.04 |
| Der p 40 (thioredoxin-like) | 12 | - | 1.10 ± 0.76 |

2.3.5 Interaction of HDM-MWCNTs with lung fluid proteins

The results above describe the protein corona formed when HDM proteins adsorb on the surface of MWCNTs. The most relevant human exposure to these HDM-MWCNT complexes is through inhalation. To probe this exposure mechanism, we investigated the interaction of BALF with MWCNTs and HDM-MWCNTs. As a first step, we confirmed that a BALF corona formed on pristine MWCNTs. Gel electrophoresis and a protein concentration assay were used to analyze the composition and concentration of the BALF protein corona (Fig. 4). A BALF corona concentration of 35.3 ± 0.85 μg protein per mg MWCNT was measured. Albumin (69 kDa) was the most

abundant protein in BALF and in the BALF corona (BALF-MWCNT) in agreement with previous work using proteomics to characterize the protein corona formed on MWCNTs incubated with BALF (24 h, 37 °C, 0.1% Pluronic).¹²³ At high BALF concentrations, two other bands are visible in both BALF and the BALF corona at ~15 kDa and ~8 kDa, along with a low molecular weight smear.

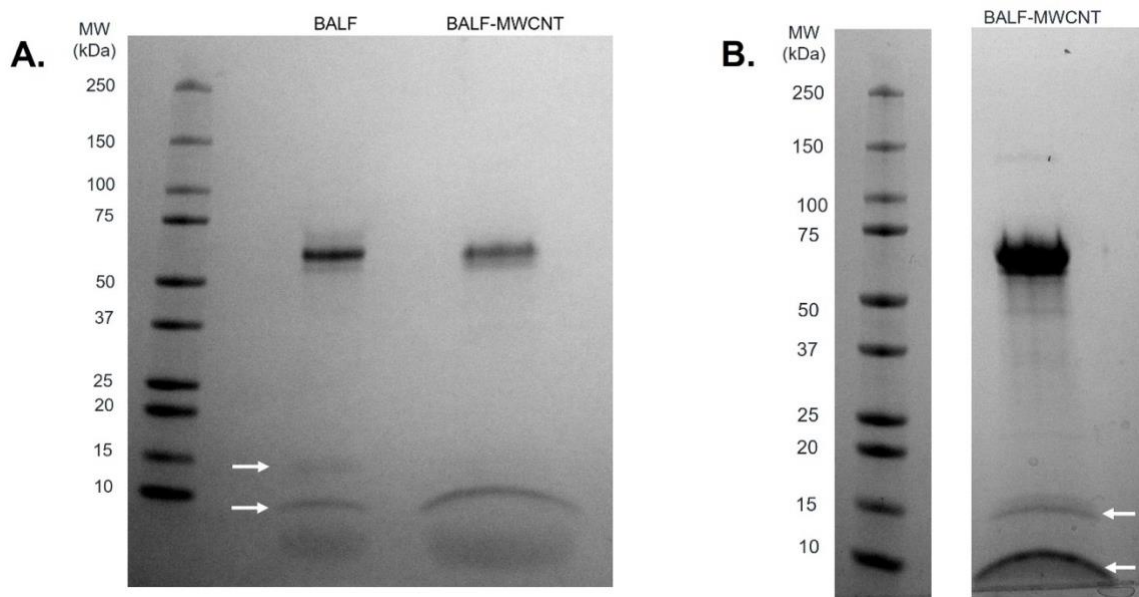


Figure 2-4: Gel electrophoresis shows the proteins present in BALF and a corona formed from BALF (BALF-MWCNT). A. Albumin is visible at 69 kDa. Bands at ~15 kDa and ~8 kDa are highlighted with arrows. B. A highly concentrated BALF-MWCNT sample makes the bands at ~15 kDa and ~8 kDa visible (arrows).

We then investigated the interaction of BALF with HDM-MWCNTs. For these experiments, we formed sequential protein coronas by first preparing HDM-MWCNTs and then incubating the HDM-MWCNTs with BALF to form an HDM-BALF-MWCNT corona (Fig. 5). Although the reverse corona (BALF-HDM-MWCNT) is less likely to be

formed in a realistic setting, we also generated these coronas for comparison. Gel electrophoresis was used to visualize these sequential coronas (Fig. 6).

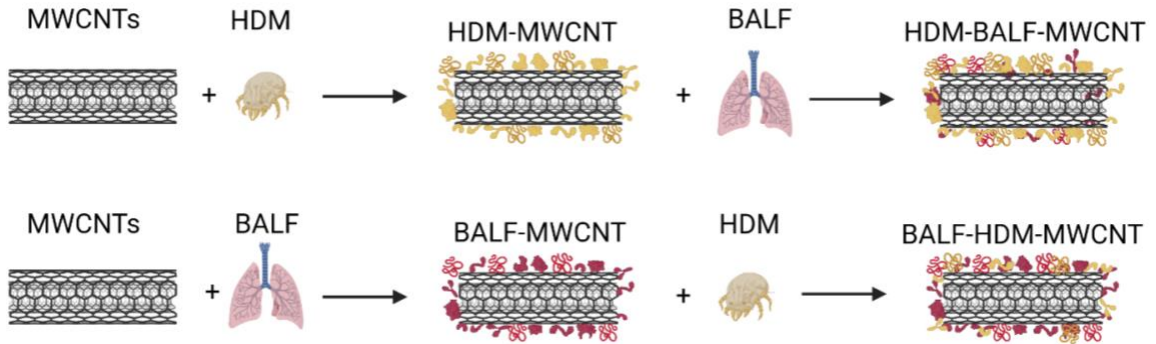


Figure 2-5: Schematic showing the formation of sequential coronas formed from HDM and BALF incubated with MWCNTs. The protein listed first is the initial protein used to form the corona.

Gel electrophoresis shows that an initial HDM corona on MWCNTs will result in a HDM-BALF-MWCNT corona with a band at ~70 kDa (likely albumin), as well as ~15 kDa and ~8 kDa (Fig. 6). A 12 kDa, possibly der p 30, is very faint. An initial BALF corona results in a BALF-HDM-MWCNT corona with similar bands to HDM-BALF-MWCNT, but different relative intensities (Fig. 6). The ~15 kDa band dominates HDM-BALF-MWCNT and the ~70 kDa band dominates BALF-HDM-MWCNT.

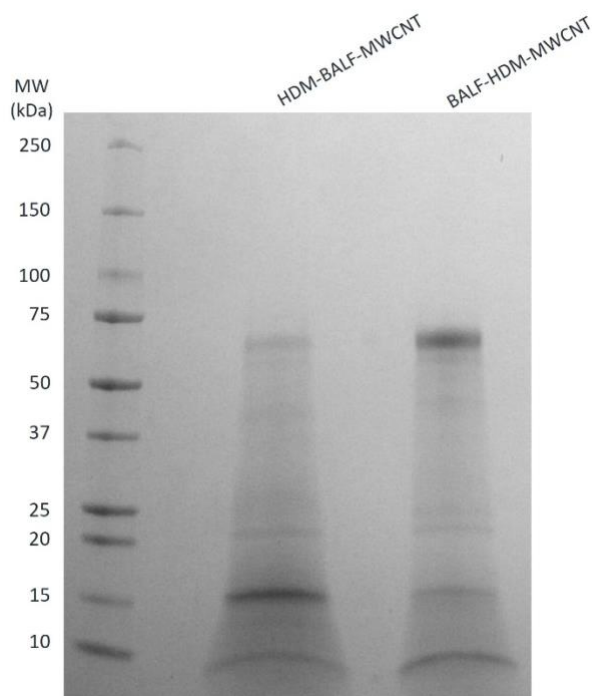


Figure 2-6: Gel electrophoresis was used to compare the proteins present in coronas formed sequentially from HDM and BALF (HDM-BALF-MWCNT and BALF-HDM-MWCNT). The protein listed first is the initial protein used to form the corona.

2.3.6 Interaction of HDM-MWCNTs with albumin

Gel electrophoresis following the incubation of HDM-MWCNTs with BALF suggests that der p 2 is present in the HDM-BALF-MWCNT coronas and is not displaced from the surface of MWCNTs by the proteins present in BALF (Fig. 6). To probe this observation, we used albumin, specifically bovine serum albumin (BSA, 66 kDa), as a representative BALF protein. The use of this single representative protein, instead of the BALF mixture, makes proteomics tractable. Repeating the formation of sequential coronas, now using BSA in place of BALF, shows a similar result. An initial HDM corona leads to a HDM-dominated corona (bands at ~15 kDa and ~12 kDa) with a

faint ~70 kDa band. An initial BSA corona leads to a complex corona dominated by a ~70 kDa band and previously unobserved proteins (Fig. 7). Der p 2 (14 kDa) is not clearly visible in the BSA–HDM–MWCNT sample.

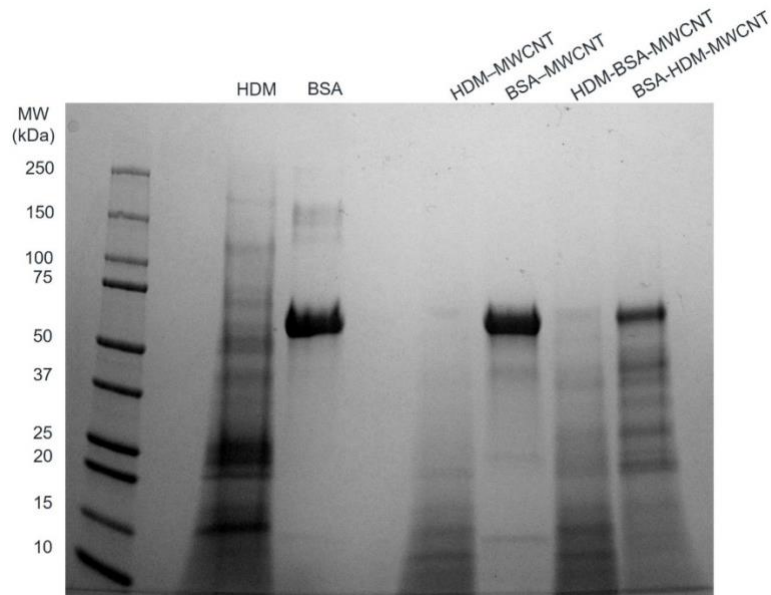


Figure 2-7: Gel electrophoresis was used to compare the proteins present in HDM alone, BSA alone, a HDM corona, a BSA corona, and sequential coronas. The protein listed first is the initial protein used to form the corona.

The proteomics data shows that the HDM–BSA–MWCNT corona contains a high concentration of albumin ($39.7 \pm 4.38\%$) and der p 2 ($36.0 \pm 2.91\%$) (Table 3, Fig. 8). Der p 30 is present at low levels ($0.781 \pm 0.81\%$). These results with BSA are in good agreement with the BALF gel electrophoresis experiments (HDM–BALF–MWCNT; Fig. 6), which showed a strong band at ~15 kDa, similar to the molecular weight of der p 2 (14 kDa) and no clear der p 30 band (12 kDa).

The BSA–HDM–MWCNT corona is less physiologically relevant as we expect the MWCNTs to be exposed to HDM and then lung fluid. The initial exposure to BSA leads to an albumin-dominated corona ($98.1 \pm 0.72\%$) with a unique collection of HDM corona proteins (Table 3). Der p 2 was not detected in the BSA–HDM–MWCNT coronas, suggesting albumin inhibits the binding of der p 2 binding to the MWCNT surface. This points towards potential surface treatments for MWCNTs that could mitigate any enhanced allergic response. The BALF–HDM–MWCNT gel electrophoresis did show a band at ~ 15 kDa, but it is likely that this is a BALF protein (Fig. 4).

Table 2-3: Normalized abundance (% of total protein) of top-5 proteins identified in HDM-BSA-MWCNT and BSA-HDM-MWCNT coronas. Proteins are ordered by abundance in HDM-BSA-MWCNT. Proteins present in a sample, but not in the top-5, are shown in italics. Proteins with normalized abundance < 0.1% are not shown. The most abundant protein is bolded. Mean and standard deviation are reported (n=3). For allergens, the biochemical name from the WHO/IUIS database is provided in parentheses.

| Protein | MW (kDa) | HDM-BSA-MWCNT (%) | BSA-HDM-MWCNT (%) |
|--|-----------|------------------------------------|------------------------------------|
| Albumin | 69 | 39.7 ± 4.38 | 98.1 ± 0.72 |
| Der p 2 (NPC2 family) | 14 | 36.0 ± 2.91 | <i>0.129 ± 0.10</i> |
| Der f 22 (Group 2-like) | 18 | 4.37 ± 6.44 | - |
| Fatty acid-binding protein-like | 15 | 3.52 ± 1.75 | - |
| Nucleoside diphosphate kinase | 18 | 2.82 ± 1.76 | - |
| Der p 30 (ferritin) | 12 | <i>0.781 ± 0.81</i> | 0.293 ± 0.50 |
| Probable methylmalonate-semialdehyde dehydrogenase | 59 | - | 0.293 ± 0.32 |
| Der p 11 (paramyosin) | 102 | <i>1.15 ± 0.61</i> | 0.129 ± 0.02 |
| Probable serine/threonine-protein kinase | 191 | - | 0.130 ± 0.084 |

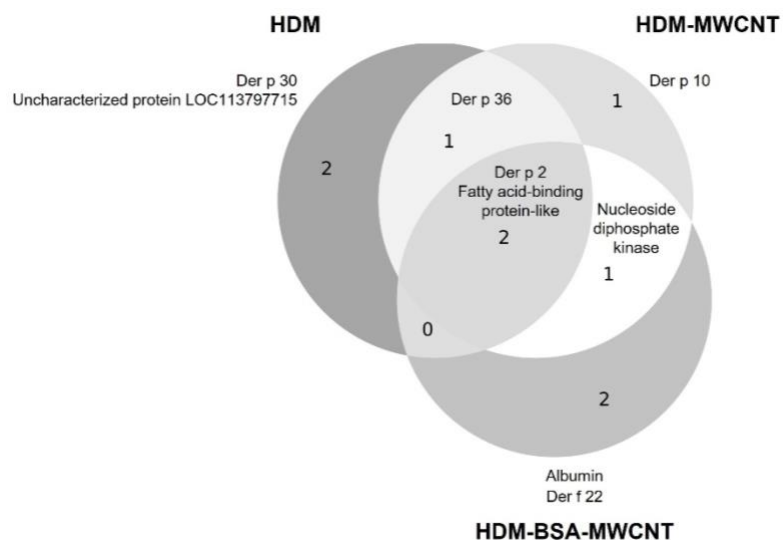


Figure 2-8: A Venn diagram shows the overlap of the top-5 proteins present in HDM extract alone, HDM-MWCNTs, HDM-BSA-MWCNTs. The two common proteins in all three samples are der p 2 and fatty acid-binding protein-like.

2.4 Conclusions

This work aimed to model real-world exposures to MWCNTs by considering the interaction of HDM proteins with MWCNTs. A combination of XPS (Table 2-1), gel electrophoresis (Figure 2-2), protein concentration assay (Figure 2-3), western blotting (Figure 2-10), and proteomics (Table 2-2, Table 2-4, and

Table 2-5) shows that HDM proteins adsorb on the surface of MWCNTs forming a protein corona, similar to the coronas observed for nanomaterials used in biomedical applications.^{47,48,124,125} Much previous work has focused on serum proteins. The protein corona dictates the subsequent biological response to these nanomaterials. It is likely that the HDM corona will similarly determine the cellular and *in vivo* response to HDM-MWCNTs. We find that der p 2, a major HDM allergen,⁹⁷ becomes highly concentrated

on the surface of MWCNTs, which may be important for allergic airway disease. When the HDM–MWCNTs are then exposed to BALF or BSA (Figure 2-5), which serves as a representative lung fluid protein, we find that der p 2 remains highly abundant ($36.0 \pm 2.91\%$ with BSA) (Figure 2-6, Figure 2-7, Table 2-3). This shows that der p 2 is not displaced from the surface of MWCNTs by lung fluid proteins and suggests that any physiological response due to the highly concentrated der p 2 will not be mitigated by lung fluid, although future functional assays will be necessary to probe the allergic potential of der p 2 adsorbed on the surface of MWCNTs. Previous *in vivo* experiments showed that mice co-exposed to MWCNTs and HDM extract displayed increased eosinophilic lung inflammation that was not observed with MWCNTs or HDM alone,¹²⁶ suggesting der p 2 is functional. The results described in this manuscript suggest that the high local concentration of der p 2 on the MWCNTs may deliver the allergen to immune cells exacerbating allergic lung inflammation. Future work will extend these studies to MWCNTs following common purification methods and chemical functionalizations to determine if these results are general. In addition, a variety of carbon-based nanomaterials present in the environment (ultrafine particulate matter, wildfire smoke) exacerbate asthma.^{127,128} Our findings may have broad implications for understanding the underlying mechanism.

2.5 Supplementary material

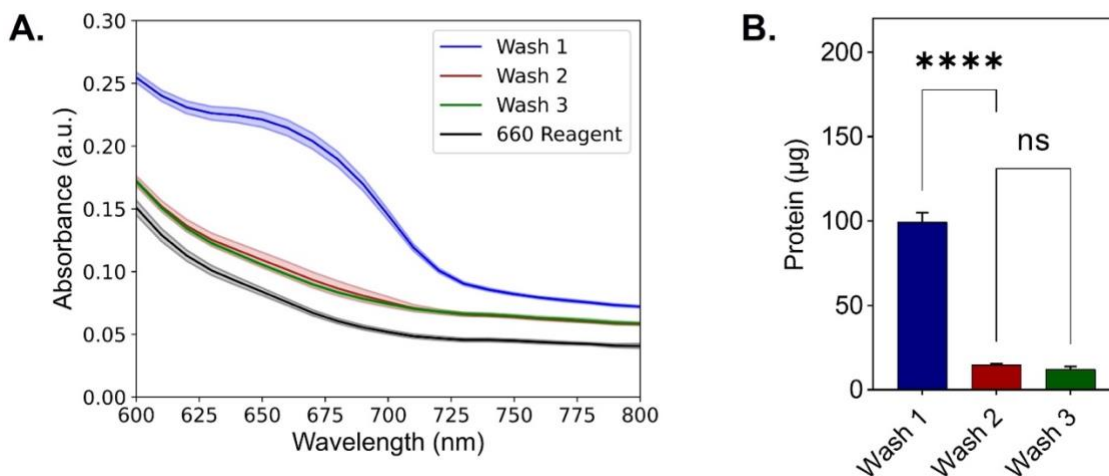


Figure 2-9: Removal of unbound HDM, referred to as washing, consisted of centrifugation, removal of supernatant, and resuspension in PBS. A. Protein concentration of the supernatant was measured with a colorimetric assay (660 nm protein assay). Solid line shows the average absorbance spectrum. Shading shows standard deviation. (n=3 distinct samples). B. The majority of the unbound HDM is removed in the first wash. Three wash steps are used to ensure all unbound protein is removed. The background signal from the 660 nm reagent was subtracted from each sample prior to calculating protein concentrations. Significance was calculated using an ANOVA with a post-hoc Tukey test. *p < 0.001, ns = not significant.

Table 2-4: Spectral counts, reported as a percent of total signal, for the excised 15 kDa band of the HDM-MWCNT corona. Proteins with spectral counts >1% are listed.

| Protein | MW (kDa) | 15 kDa (%) |
|---|----------|------------|
| Der p 2 (NPC2 family) | 14 | 81.6 |
| Thioredoxin | 12 | 9.70 |
| Der p 36 (C2 domain containing protein) | 25 | 3.51 |
| Nucleoside diphosphate kinase | 18 | 1.56 |

Table 2-5: Spectral counts, reported as a percent of total signal, for the excised 12 kDa band of the HDM-MWCNT corona. Proteins with spectral counts >1% are listed.

| Protein | MW (kDa) | 12 kDa (%) |
|--|----------|------------|
| Der p 30 (ferritin) | 12 | 71.0 |
| Fructose-bisphosphate aldolase | 39 | 9.84 |
| Der p 11 (paramyosin) | 102 | 5.22 |
| Uncharacterized protein LOC113797715 | 191 | 4.71 |
| Glutathione peroxidase | 25 | 1.88 |
| Myosin heavy chain | 112 | 1.73 |
| Inosine-5'-monophosphate dehydrogenase | 56 | 1.51 |

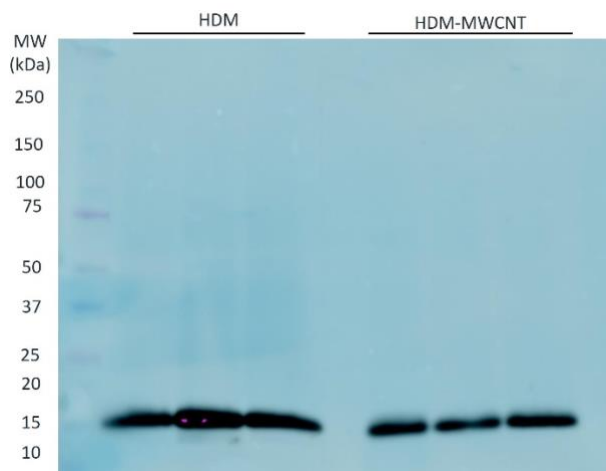


Figure 2-10: Western blotting using an antibody against der p 2 confirms the band visible at ~15 kDa is der p 2 (14 kDa).

Table 2-6: Normalized abundance (% of total protein) of the top-10 proteins identified in HDM and the HDM corona formed on MWCNTs (HDM-MWCNT). Proteins present in a sample, but not in the top-10, are shown in italics. Proteins with normalized abundance < 0.1% are not shown. The most abundant protein in each sample is bolded. Mean and standard deviation are reported (n=3). A different lot (#390991) of HDM was used in comparison to the data in the main text (Table 2). For both lots, der p 2 is the most abundant protein in corona.

| Protein | MW (kDa) | HDM (%) | HDM-MWCNT (%) |
|--------------------------------------|----------|--------------------|--------------------|
| Der p 2 (NPC2 family) | 14 | 24.5 ± 5.20 | 51.6 ± 15.6 |
| Der p 1 (cysteine protease) | 34 | 23.6 ± 0.98 | 4.72 ± 3.69 |
| Der p 30 (ferritin) | 12 | 8.50 ± 2.62 | 4.22 ± 1.17 |
| Uncharacterized protein LOC113799616 | 25 | 7.28 ± 2.31 | 10.7 ± 9.76 |
| Uncharacterized protein LOC113797715 | 191 | 7.04 ± 2.13 | <i>0.71 ± 0.29</i> |
| Uncharacterized protein LOC113790193 | 27 | 3.48 ± 1.80 | 3.12 ± 1.67 |
| Fatty acid-binding protein-like | 15 | 2.19 ± 0.39 | 2.76 ± 2.48 |
| Nucleoside diphosphate kinase | 18 | 1.91 ± 0.82 | 3.92 ± 1.78 |
| Uncharacterized protein LOC113796509 | 77 | 1.85 ± 1.80 | - |
| Der p 10 (tropomyosin) | 33 | 1.28 ± 1.07 | <i>0.74 ± 0.85</i> |
| Der f 22 (Group 2-like) | 18 | <i>0.47 ± 0.77</i> | 3.35 ± 3.32 |
| Der p 11 (paramyosin) | 102 | 0.25 ± 0.056 | 1.96 ± 1.57 |
| Lysosomal aspartic protease-like | 45 | <i>0.13 ± 0.19</i> | 1.09 ± 1.84 |

3. Enzyme activity of cysteine and serine proteases adsorbed on to nanomaterials

HDM, one of the main sources of Type 1 allergies around the world, is made up of various proteins and allergens.¹²⁹ These allergens are characterized into groups containing related homologs. Allergen groups are comprised of different types of proteases. Group 1 allergens consist of cysteine proteases, such as Der p 1. Group 3 allergens are made up of serine proteases like Der p 3. We investigate the interactions of HDM proteases with MWCNT to assess the implications of HDM and MWCNT co-exposures. We used a casein-based fluorescence protease assay to quantify the concentrations of enzymes in HDM, HDM and MWCNT mixtures, and HDM-MWCNT coronas. Isolated cysteine and serine protease interactions with MWCNTs were investigated by comparing the enzyme concentration of papain-MWCNTs against free papain and trypsin-MWCNT against free trypsin. We also analyzed trypsin and papain interactions with PS NPs. We found that there was more proteolytic activity in free enzyme samples was higher compared enzyme-MWCNT coronas, including HDM, trypsin and papain. The same results were found for enzyme-PS coronas. These results could be a result of partial enzyme denaturation following adsorption on to MWCNTs or PS NPs.

3.1 Introduction

Protein interactions with nanomaterials have been studied extensively, and it is well known that protein adsorbing onto the surface of nanomaterials results in the

formation of a protein corona.^{47,48,85,130} Enzymes adsorption on the nanomaterials has also garnered scientific interest due to the biocatalytic characteristics of active enzymes.¹³¹ Adsorption of enzymes on nanomaterials, often referred to as enzyme immobilization, can be used for a wide range of applications. Nanomaterials can be utilized as nanocarriers that support, stabilize, and manipulate the biocatalytic efficiency of enzymes.¹³² The size, structure, surface charge, and functionalization of a nanomaterial dictates whether enzyme activity will be inhibited or enhanced.^{133,134} Additionally, the size, orientation, and active site location are enzyme characteristics that previous studies have found to affect adsorption and activity of enzymes on mesoporous silica.¹³⁵⁻¹³⁷

CNTs have been a nanomaterial of interest due to their optical and mechanical properties.¹³⁸ The environmental effects of CNTs have caused researchers to investigate the degradation of CNTs using enzymes.¹³⁹ Horseradish peroxidase has been found to remain active after adsorption onto the surface of CNTs and degrade single and MWCNTs.¹⁴⁰⁻¹⁴² The catalytic reaction causing degradation was driven by the functionalization of the CNTs and the enzyme structure.

We previously analyzed the composition of an HDM protein corona on MWCNT in Chapter 3.¹⁴³ HDM are composed of various proteins and proteases that cause allergic airway disease, such as allergies. The HDM allergens *Dermatophagoides pteronyssinus* (Der p) 1, 3, 6 and 9 are cysteine and/or serine proteases are the main proteins that contribute to allergic inflammation.¹⁴⁴ Quantifying the proteolytic activity of HDM after adsorption onto MWCNTs provides insight to the biological effects of HDM-

MWCNT interactions. To further understand how enzymes interact with MWCNTs, we investigate the interactions of MWCNTs with papain, a cysteine protease, and trypsin, a serine protease. The enzymatic activity of papain and trypsin after interactions with carboxylated PS NPs is also of interest. Overall, we aim to understand how cysteine and serine protease interact with MWCNTs and PS NPs.

3.2 *Materials and Methods*

3.2.1 Nanoparticle (NP) preparation

MWCNTs (NC7000, Nanocyl, Sambreville, Belgium) and cationic-modified PS NPs (0.2 μm , #37356, Thermo Fisher, Waltham, MA) were used for all experiments. Stock solutions of MWCNTs were prepared by suspending dry MWCNTs (10 mg/mL) in 1X phosphate buffered saline (PBS; 21300025, Thermo Fisher). Solutions were sonicated for five minutes with a cup horn sonicator (40% amplitude; Q500 Sonicator, Q Sonica, Newtown, CT) to help suspend the MWCNTs. Polystyrene stock solutions were briefly vortexed prior to use.

3.2.2 Preparing protein mixtures and coronas

The proteins used in experiments included house dust mite serum (*Dermatophagoides pteronyssinus*, XPB91D3A2.5, Lot 414145, Stallergenes Greer, Lenoir, NC), papain from papaya latex (P3125, Sigma Aldrich, Saint Louis, MO), bovine serum albumin (BSA; A2153-50G, Sigma-Aldrich, St. Louis, MO), and L-1-tosylamido-2-phenylethyl chloromethyl ketone (TPCK) treated trypsin (#20233, Thermo Fisher). The

HDM and MWCNT mixture was prepared by combining HDM and MWCNTs and briefly vortexing the samples. The protein corona formation method on MWCNTs has been described previously in Chapter 2. Proteins were incubated with either MWCNTs or PS NPs for 30 minutes at room temperature (RT) on an orbital shaker (700 rpm, 88882006, Digital Microplate Shaker, Thermo Fisher). Corona samples were washed three times by centrifugation (15-30 minutes, 4°C, 14,000 RPM) to remove unbound proteins and resuspended in PBS.

3.2.3 Protein concentration and proteolytic activity

The concentration of protein adsorbed on the NPs was measured using a colorimetric assay, called the BCA Protein Assay (#23227, Thermo Fisher). Enzyme activity of corona and free protein samples were measured using a fluorescent protease assay (#23266, Thermo Fisher). Absorbance and fluorescence of samples was measured using a plate reader (SpectraMax iD3, Molecular Devices, San Jose, CA).

3.3 Results and Discussion

3.3.1 Proteolytic activity of HDM and MWCNTs

The proteolytic activity following the interactions between HDM and MWCNTs were quantified by comparing the concentration of enzymes in HDM, a mixture of HDM and MWCNTs, and a HDM corona on MWCNTs using a fluorescent protease assay (Figure 3-1). To form the corona, HDM (1 mg/mL) was incubated with MWCNTs (1 mg/mL) for 30 minutes at RT, and washed by centrifugation x3, as described in the

Materials and Methods. The mixture was prepared by combining HDM (1 mg/mL) with MWCNTs (1 mg/mL). HDM matched the concentration of the corona, which was reported in our previous paper.¹⁴⁵ The mixture had the highest amount of enzyme activity with 76.2 ± 6.45 $\mu\text{g/mL}$ of enzymes, followed by HDM with 60.8 ± 1.12 $\mu\text{g/mL}$ of enzymes. The HDM-MWCNT samples had the lowest concentration of enzymes with 25.3 ± 4.00 $\mu\text{g/mL}$ of enzymes. HDM is comprised of various proteins, which includes protease allergens.⁹⁶ Group 1 allergens, such as Der p 1, are papain-like cysteine proteases with high amounts of proteolytic activity.^{96,146} We previously reported that Der p 1 and Der p 2, a group 2 allergen, are within the top-10 proteins present in HDM.^{145,147} In the same study, we found that an HDM-MWCNT corona was dominated by Der p 2 but had a low abundance of the highly proteolytic Der p 1.¹⁴³ The low concentration of Der p 1, a proteolytic protein, in HDM-MWCNT coronas provides an explanation for the low concentration of enzyme activity measured, compared to HDM and the mixture, which have a higher abundance of Der p 1 (Figure 3-1B).

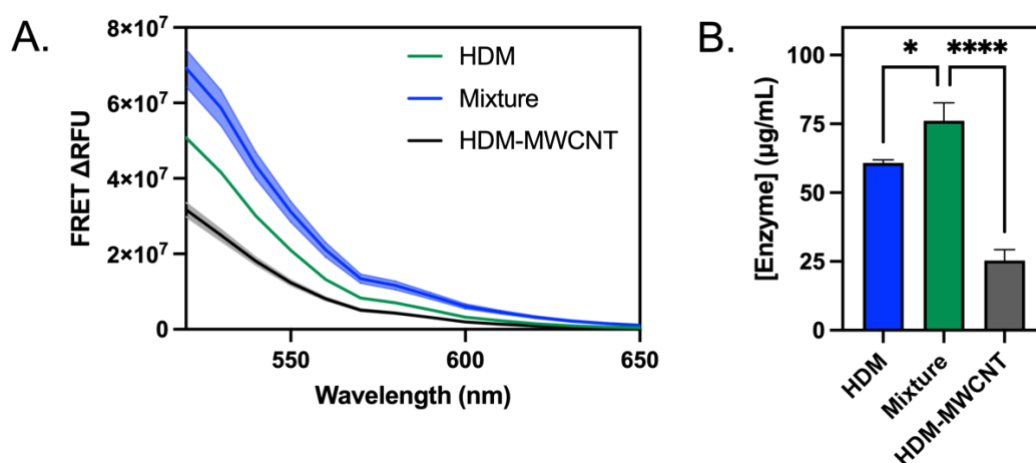


Figure 3-1 Comparing the proteolytic activity of HDM, mixture of HDM and MWCNT, and an HDM corona on MWCNTs. (A) MWCNTs (1 mg mL^{-1}) were incubated with HDM (1 mg mL^{-1}). The enzyme activity of the free protein, mixture and corona were measured with a fluorescent enzyme assay (Pierce Fluorescent Protease Assay; $n=3$ distinct samples). Solid lines show the mean and shading shows the standard deviation. (B) Enzyme activity of the resulting corona compared to free HDM and mixture. Significance was calculated using an ANOVA with a post-hoc Tukey test. * $p < 0.1$, ** $p < 0.0001$**

3.3.2 Concentration of enzyme coronas on MWCNTs

We measured the proteolytic activity of other enzyme coronas on MWCNTs. The concentration of trypsin and papain adsorbed onto MWCNTs was quantified using a colorimetric BCA assay (Figure 3-2A, B). The concentration of trypsin on MWCNTs (trypsin-MWCNT) was similar to the concentration of papain on MWCNTs (papain-MWCNT, Figure 3-2C). Trypsin-MWCNT coronas had a protein concentration of $53.5 \pm 9.63 \mu\text{g mg}^{-1}$ MWCNT, and papain-MWCNT coronas had a protein concentration of $48.3 \pm 25.1 \mu\text{g mg}^{-1}$ MWCNT. The adsorption of papain and trypsin is a higher concentration than previously reported for HDM adsorbed on MWCNT.¹⁴³ In comparison, non-enzyme coronas, such as human platelet proteins, contained a higher concentration of

proteins on the surface of carboxyl functionalized CNTs. For example, the concentration of immunoglobulin G coronas was $9.66 \pm 0.11 \text{ nmol mg}^{-1} \text{ CNTs}$.¹⁴⁸

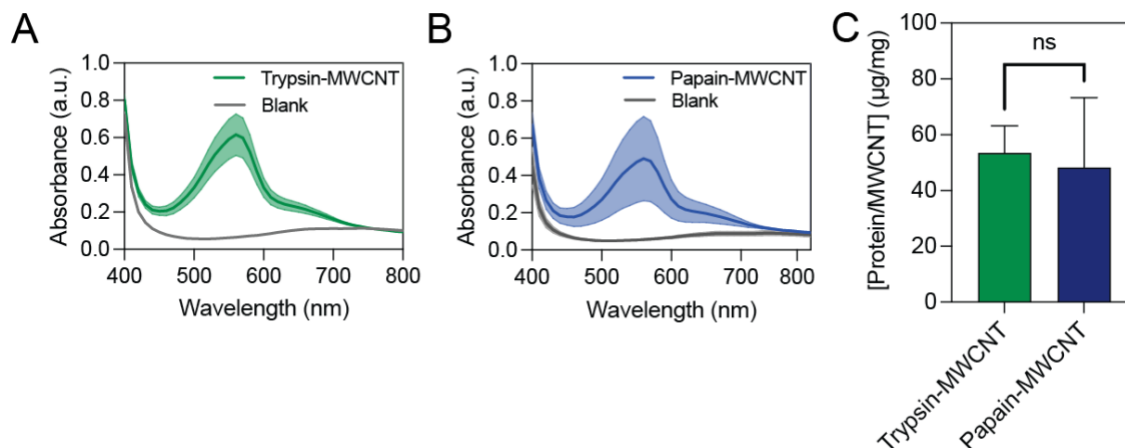


Figure 3-2: Protein concentrations of enzyme coronas on MWCNTs. MWCNTs (1 mg mL^{-1}) were incubated with (A) trypsin (1 mg mL^{-1}) or (B) papain (1 mg mL^{-1}). The protein concentration was measured with a colorimetric protein assay (BCA assay; $n=3$ distinct samples). Solid lines show the mean and shading shows the standard deviation. (C) Protein concentration of the resulting coronas. Significance was calculated using an ANOVA with a post-hoc Tukey test. ns = not significant.

3.3.3 Concentration of active enzymes on MWCNT coronas compared to free enzymes

The results above describe the concentration of enzymes adsorbed onto the surface of MWCNTs. As the protein corona dictates the biological identity of the MWCNTs, it is important to characterize the inhibition or enhancement of enzyme activity following the enzymatic adsorption onto the nanomaterials. The enzymatic activity can be affected by the physical properties of the nanomaterial and the type or orientation of enzymes.¹⁴⁹ To characterize the enzymatic activity of trypsin and papain on the surface of MWCNTs, a fluorescent protease assay was used to compare the

activity of free enzymes to the activity of an enzyme corona. The concentration of free trypsin and papain was matched to the concentration of the enzyme adsorbed onto MWCNTs, as measured using a BCA assay (Figure 3-2). We compared the concentration of active enzymes in free trypsin to the active enzymes in trypsin-MWCNT (Figure 3-3A). The enzymatic activity of trypsin adsorbed onto MWCNTs is significantly inhibited compared to free trypsin (Figure 3-3B). Papain enzyme activity was also inhibited when adsorbed onto MWCNTs, compared to free papain (Figure 3-3C, D). The decrease in enzyme activity from trypsin-MWCNT and papain-MWCNT can be explained by examining the nature of enzyme-nanomaterial interactions. Nanomaterial and enzyme interactions often lead to enzyme activity inhibition. One of the ways this can occur is if the enzyme active site binds to the surface of the nanomaterials, which blocks the enzyme from interacting with substrates.^{132,133} Nanoparticle surface characteristics can also affect enzyme activity. Hydrophobic materials, like non-functionalized MWCNTs, can act as effective enzyme inhibitors.^{133,150} For example,

adsorption of catalase on hydrophobic CNTs can cause the enzymes to denature.¹⁵¹

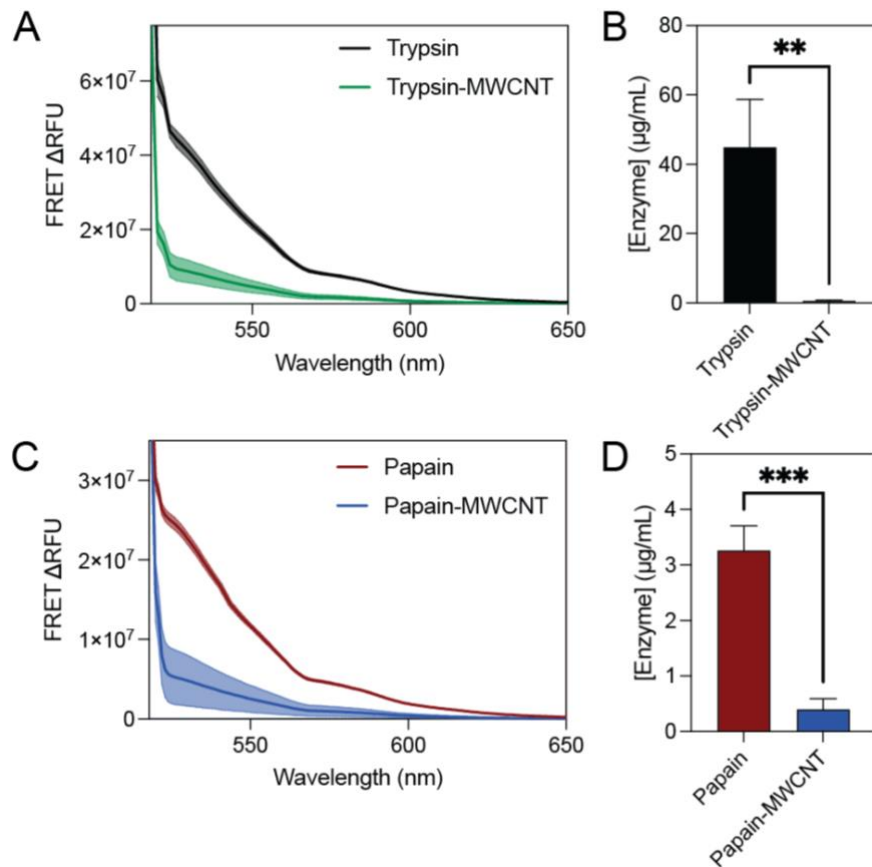


Figure 3-3: Comparing the proteolytic activity free enzymes and enzyme coronas on MWCNTs. MWCNTs (1 mg/ml) were incubated with (A) trypsin (1 mg mL⁻¹) or (C) papain (1 mg mL⁻¹). The enzyme activity of the free protein, mixture and corona were measured with a fluorescent enzyme assay (Pierce Fluorescent Protease Assay; n=3 distinct samples). Solid lines show the mean and shading shows the standard deviation. (B) Active enzyme concentration of free trypsin compared to trypsin-PS. (D) Active enzyme concentration of free papain compared to papain-PS. Significance was calculated using a t-test. ** $p < 0.01$, *** $p < 0.001$, **** $p < 0.0001$

3.3.4 Concentration of enzyme coronas on PS NPs

The interactions between enzymes and nanomaterials were further studied by examining the adsorption of trypsin and papain on PS NPs. The concentration of trypsin and papain adsorbed on to the surface of PS NPs was quantified used a BCA assay

(Figure 3-4). Trypsin and papain adsorbed at a similar concentration on PS. Trypsin-PS coronas had a protein concentration of $37.4 \pm 2.87 \mu\text{g mg}^{-1}$ PS and papain-PS coronas had a protein concentration of $31.4 \pm 3.31 \mu\text{g mg}^{-1}$ PS. The similarity in concentration suggest that the adsorption capacity for trypsin and papain is relatively equal. Previous studies have demonstrated the adsorption capacity on PS NPs can differ depending on the enzyme. For example, pepsin and α -amylase adsorb on PS at similar concentrations. In comparison, trypsin was found to adsorb at a concentration 6x less than pepsin and α -amylase.¹⁵² Additionally, there can be variance in enzyme adsorption depending on the characteristics of the nanomaterial. A past study found that the adsorption of trypsin on magnetic $\text{Fe}_3\text{O}_4@\text{SiO}_2$ was $65 \mu\text{g mg}^{-1}$ of $\text{Fe}_3\text{O}_4@\text{SiO}_2$ NPs.¹⁵⁰

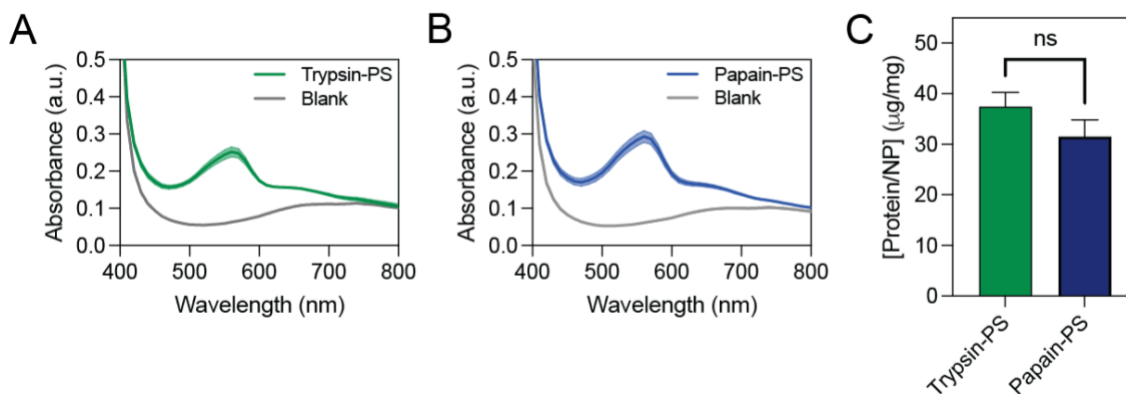


Figure 3-4: Protein concentrations of enzyme coronas on PS compared to BSA coronas on PS. PS NPs (1 mg mL^{-1}) were incubated with either (A) trypsin (1 mg mL^{-1}) or (B) papain (1 mg mL^{-1}). The protein concentration was measured with a colorimetric protein assay (BCA assay; $n=3$ distinct samples). Solid lines show the mean and shading shows the standard deviation. (C) Protein concentration of the resulting corona. Significance was calculated using a t-test. ns = not significant

3.3.5 Concentration of active enzymes on PS enzyme coronas compared to free enzymes

We measured the concentration of active enzymes in trypsin-PS and papain-PS and compared the activity of the free coronas the free enzyme (Figure 3-5). The results from the protease assay demonstrated that the trypsin and papain are more active in solution than adsorbed onto PS NPs. Enzyme activity after interactions with PS and MWCNTs have shown to result in an inhibited enzyme corona. The inhibition of papain on PS and MWCNTs can be attributed to the cystine side chain active site, which can become easily blocked and cause the enzyme to denature.¹⁵³ Trypsin activity is affected by a different mechanism. The ratio between trypsin and NPs present during an interaction can affect enzyme activity, such that higher concentrations of NPs can damage the conformation of the protein.^{154,155} Overall, we can conclude that the higher concentration of activity in free enzymes, compared to enzyme coronas, is due to the structure and concentration of enzymes to NPs.

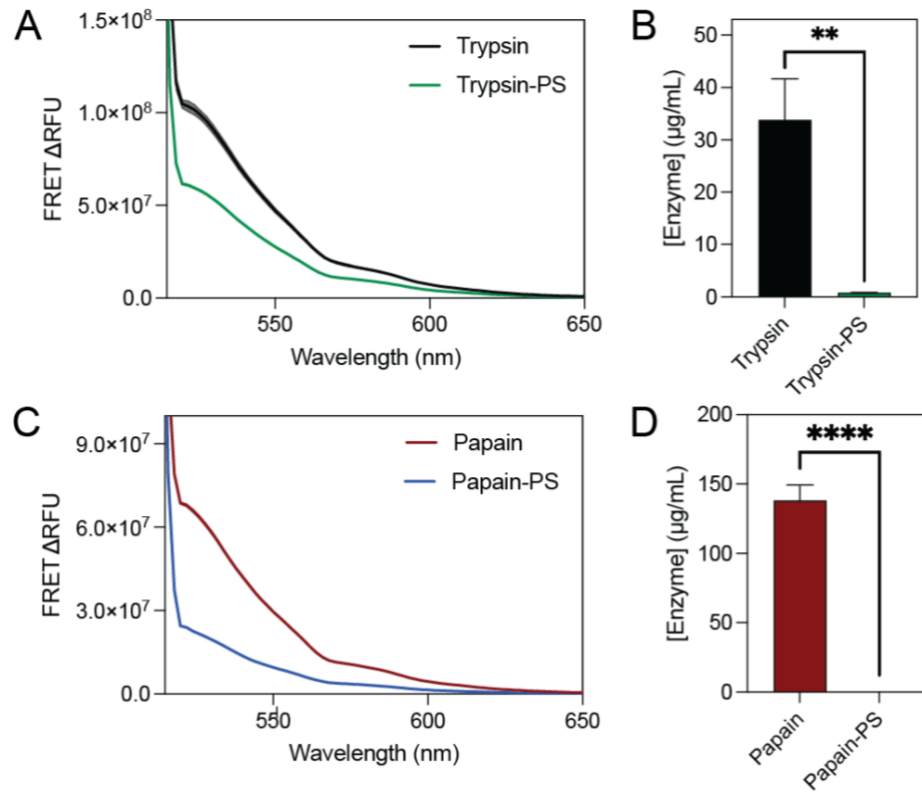


Figure 3-5: Comparing the proteolytic activity free enzymes and enzyme coronas on PS nanoparticles. PS (1 mg/ml) was incubated with (A) trypsin (1 mg/mL) or (C) papain (1 mg/mL). The enzyme activity of the free protein, mixture and corona were measured with a fluorescent enzyme assay (Pierce Fluorescent Protease Assay; n=3 distinct samples). Solid lines show the mean and shading shows the standard deviation. (B) Active enzyme concentration of free trypsin compared to trypsin-PS. (D) Active enzyme concentration of free papain compared to papain-PS. Significance was calculated using a t-test. ** $p < 0.01$, **** $p < 0.0001$

3.4 Conclusions

This work analyzes the interactions between cysteine and serine protease and nanomaterials. Our experiments aim to model a MWCNT manufacturing setting, in which interactions between HDM and MWCNTs are highly probable. We quantified the active enzyme concentration of HDM, a serum consisting various proteins including cysteine and serine proteases, when free in solution, mixed with MWCNTs, and

adsorbed on to the surface of MWCNTs (Figure 3-1). The results from this comparison showed that a mixture of HDM and MWCNTs, at equal concentrations, contained the highest concentration of active enzymes. HDM-MWCNT contained the lowest concentration of active enzymes. Cysteine and serine proteases in HDM are responsible for allergic inflammation.¹⁵⁶⁻¹⁵⁸ A decrease in protease activity indicates that adsorption of HDM onto MWCNTs will not exacerbate allergic airway diseases caused by HDM proteins.

Isolated cysteine and serine protease interactions with MWCNTs were investigated by comparing the active concentration enzyme concentration of papain-MWCNTs against free papain and trypsin-MWCNT against free trypsin (Figure 3-3). A higher concentration of active enzymes was measured for the free enzyme samples compared to the low concentrations of active enzymes in the enzyme-MWCNT coronas. Replacing the nanomaterial with PS to determine if the low concentration of active enzymes in MWCNTs coronas was due to materials, resulted in similar results to those of enzyme-MWCNTs (Figure 3-5). The lack of high enzyme activity in both enzyme-MWCNT and enzyme-PS coronas was likely due to the structure of papain and trypsin enzymes. The future direction of enzyme-MWCNT interactions could entail using functionalized MWCNTs as the nanomaterial of interest.

4. Concentration of protein coronas on purified and functionalized MWCNTs as a function of initial protein concentration

We investigate the effects of inhaling pristine, purified, and functionalized MWCNTs by analyzing the adsorption of BSA, a representative lung fluid protein. The adsorption of HDM proteins onto pristine and purified MWCNTs was also analyzed to understand how HDM interacts with various types of MWCNTs. A colorimetric assay was used to measure the concentration of protein adsorbed onto the surface of MWCNTs. Gel electrophoresis was used to compare the composition of HDM coronas on pristine and purified MWCNTs. A linear relationship between initial BSA protein concentration and adsorption was observed only for pristine MWCNTs. The results from the purified and functionalized MWCNTs indicate that there is a possible maximum amount of protein that can adsorb onto the surface. This maximum is not the same across all the MWCNTs. HDM coronas formed on pristine, CP, and TP MWCNTs all revealed abundance of a 15 kDa protein, likely Der p 2. These findings highlight the potential influence of MWCNT surface properties on protein corona and the downstream effects of inhalation and exposure to HDM.

4.1 Introduction

Commercial scale manufacturing of MWCNTs utilizes various methods of catalytic vapor deposition. This results in MWCNTs that typically contain below 2 wt% of impurities. These impurities are remnants of transition metals used as a catalyst, such

as aluminum and nickel.⁴¹ Thermal and chemical purification processes are used to remove impurities such as amorphous carbon, multishell carbon nanocapsules, and residual catalyst metals.^{159,160} Following purification, MWCNTs can be functionalized with carboxyl or amine groups. Plasma functionalization of thermally purified (TP) MWCNTs can be used to achieve carboxyl functionalized TP MWCNTs (TP+COOH) and amine functionalized TP MWCNTs (TP+NH₂) as a relatively non-disruptive method.¹⁵⁹ Chemically purified (CP) MWCNTs can also be functionalized with carboxyl (CP+COOH) or amine (CP+NH₂) groups. These variations from pristine MWCNT are depicted in Figure 4-1.

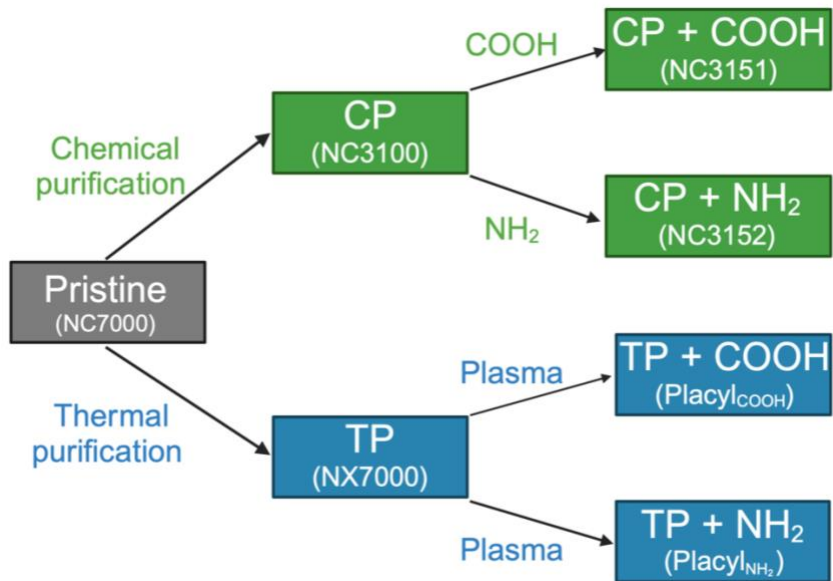


Figure 4-1: Schematic of the types of MWCNTs, including pristine, purified and functionalized varieties. The manufacturer name is included for each MWCNT in parenthesis.

As MWCNT become more widely utilized, understanding the biological implications of exposure to this nanomaterial becomes critical. Inhalation of MWCNTs is

one of the exposure pathways of primary concern. Previous studies have characterized the pulmonary toxicity of MWCNTs using animal models.^{45,60} Moreover, in a manufacturing and consumer setting, MWCNTs could encounter and interact with house dust mites (HDM). Given that HDM causes allergic airway disease, such as allergies in 1-2% of the global population, and the ubiquity of HDM in an indoor environment, further investigating the interaction between MWCNTs and HDM is important.^{161,162}

Surface functionalization can affect the hydrophobicity, polydispersity, and the protein corona of MWCNTs.^{148,163} Previous work has shown that carboxylated nanoparticles (NPs) yield a higher adsorption of proteins onto the surface.¹⁶⁴ To understand how purification and functionalization of MWCNTs interact with proteins, specifically lung fluid proteins, we incubated 7 types of MWCNTs with varying concentrations of albumin (BSA), the most abundant protein in lung fluid, and measured the concentration of BSA adsorbed. We additionally compared the concentration and composition of HDM adsorbed onto the surface of pristine and purified MWCNTs.

4.2 Materials and Methods

4.2.1 MWCNT characterization

Pristine (NC7000), purified (NC3100, NX7000), and functionalized (NC3151, NC3152, Placly_{COOH}, Placly_{NH₂}) MWCNTs (Nanocyl, Sambreville, Belgium) were used for all experiments. Stock solutions of MWCNTs were prepared by suspending dry MWCNTs (10 mg mL⁻¹) in 1X phosphate buffered saline (PBS; 21300025, Thermo Fisher).

Solutions were sonicated for five minutes with a cup horn sonicator (40% amplitude; Q500 Sonicator, Q Sonica, Newtown, CT) to help suspend the MWCNTs.

4.2.2 Protein corona formation and concentration

The protein corona formation method on MWCNTs has been described previously in Chapter 2. The proteins used in experiments included house dust mite serum (*Dermatophagoides pteronyssinus*, XPB91D3A2.5, Lot 394845, Stallergenes Greer, Lenoir, NC) and bovine serum albumin (BSA; A2153-50G, Sigma-Aldrich, St. Louis, MO). To remove unbound protein, samples were washed three times by centrifugation (15–30 minutes, 4 °C, 14 000 rpm) and resuspension in PBS. Removal of unbound and weakly bound proteins results in a “hard” corona. Protein concentrations were measured with a colorimetric assay (Pierce 660 nm Protein Assay, referred to as a 660 nm assay, 2260, Thermo Fisher Scientific) and quantified with a plate reader (SpectraMax iD3, Molecular Devices, San Jose, CA).

4.2.3 Gel electrophoresis

The compositions of the protein coronas were visualized using gel electrophoresis. Protein–MWCNT complexes were resuspended in Laemmli SDS-sample buffer (4×, reducing, BP-110R, Boston BioProducts, Milford, MA). Proteins were denatured by boiling samples at 95 °C for 5 minutes before loading into a tris-glycine sodium dodecyl sulfate (SDS) precast polyacrylamide gel (4561096, Bio-Rad Laboratories, Hercules, California). A 10–250 kDa molecular weight marker (Precision

Plus Protein Dual Color Standards, 1610374, Bio-Rad) was included in the gel. A voltage of 230 V was applied for 30 minutes. The gel was rinsed by microwaving in deionized water three times (1 minute heat, 1 minute rocking at RT, water replaced). The gel was then stained (SimplyBlue Safe Stain, LC6060, Thermo Fisher) by microwaving for 45 seconds and rocking for 5 minutes at RT. Deionized water was used to destain the gel (rocking overnight, RT) before imaging (PhotoDoc-It; Analytik Jena, Jena, Germany).

4.3 Results and Discussion

4.3.1 Albumin adsorption on pristine, purified, and functionalized MWCNTs

The concentration of BSA proteins that adsorb onto the surface of pristine, purified, and functionalized MWCNTs was quantified using a 660 protein assay (Figure 4-2). All 7 types of MWCNTs (1 mg mL^{-1}) were incubated with increasing concentrations of BSA ($0.1 - 2.0 \text{ mg mL}^{-1}$). For these experiments, incubation time was kept at 30 minutes. The resulting concentration of BSA adsorbed onto pristine MWCNTs increased linearly from $0.1 - 2.0 \text{ mg mL}^{-1}$ (Figure 4-2B). The protein increased by 11.0 ug mL^{-1} MWCNT as the concentration of BSA increases by 1 mg mL^{-1} . The other MWCNT coronas (CP, TP, CP+COOH, CP+NH₂, TP+COOH, TP+NH₂) did not follow a similar linear trend. BSA adsorbed onto CP MWCNTs was similar at lower concentrations (0.1 mg mL^{-1} to 0.5 mg mL^{-1}). There was an increase in BSA adsorption when the BSA concentration was increased from 0.1 mg mL^{-1} to 0.75 mg mL^{-1} . Adsorption between $0.75 \text{ mg mL}^{-1} - 2.0 \text{ mg mL}^{-1}$ yielded similar results. The amount of BSA adsorbed on CP

MWCNTs increases when the initial concentration of BSA concentration is increased by ~10-fold. The carboxyl functionalized CP MWCNTs results demonstrated that coronas at an initial concentration of BSA 2.0 mg mL⁻¹ contained the highest amount of protein. Initial concentrations of BSA from 0.1 – 1.5 mg mL⁻¹ yielded coronas of similar μg protein/mg MWCNT. For CP+NH₂, significant increases in protein adsorption were found when the incubation concentration was increased from 0.1 – 0.25 mg mL⁻¹ to 2.0 mg mL⁻¹. This suggest that in order to achieve a corona with a higher amount of protein on CP+NH₂, the incubation concentration must be increased by at least 8-fold. There were no observable trends in protein adsorption were identified for TP and TP+COOH at incubation concentrations from 0.1 – 2.0 mg mL⁻¹. In contrast, TP+NH₂ indicated that BSA adsorption from incubation concentrations between 0.1 – 1.0 mg mL⁻¹ were comparable, yet this group contained less protein than coronas with incubation concentration from 1.5 – 2.0 mg mL⁻¹. Overall, each type of MWCNT exhibited a different relation between incubation concentration and corona concentration. Previous studied have investigated the effects of increasing the incubation concentration on the final corona concentration.^{118,120,165,166} For example, carboxylate-modified iron oxide NPs were incubated with increasing concentrations of fetal bovine serum, which resulted in increasing corona concentrations.¹⁶⁵

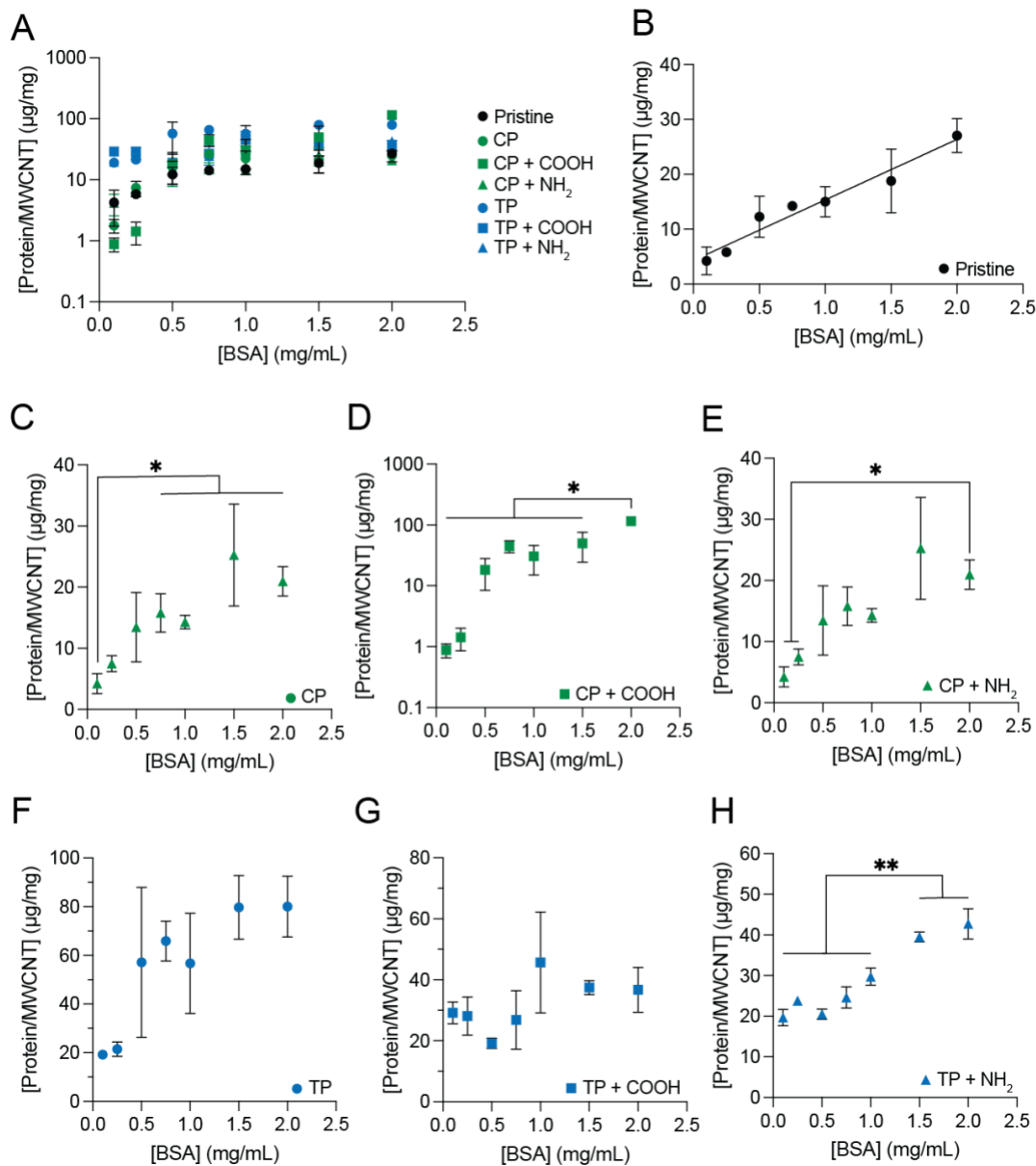


Figure 4-2: Protein concentration of the HDM corona formed on pristine, purified, and functionalized MWCNTs. (A) Comparing the concentration of a corona formed by incubating MWCNTs (1 mg mL^{-1}) were incubated with increasing concentrations of BSA ($0.25 \text{ mg mL}^{-1} - 1 \text{ mg mL}^{-1}$). The concentration of the resulting corona was measured with a colorimetric protein assay (660 nm assay; $n = 3$ distinct samples). (B) Protein concentration of the resulting (B) pristine, (C) CP, (D) CP + COOH, (E) CP + NH₂, (F) TP, (G) TP + COOH, and (H) TP + NH₂ corona. Significance was calculated using an ANOVA with a *post hoc* Tukey test. ns = not significant not shown, * $p < 0.1$, ** $p < 0.01$

4.3.2 HDM forms a corona on thermally and chemically purified MWCNTs

To further analyze the adsorption of protein on pristine, CP, and TP MWCNTs, HDM (1 mg mL^{-1}) was incubated with 1 mg mL^{-1} of MWCNTs (Figure 4-3). The concentration of HDM adsorbed onto pristine, CP, and TP MWCNTs was similar. HDM adsorbed at a range of $11 - 15 \text{ } \mu\text{g mL}^{-1}$ MWCNT between all three types of MWCNTs. As we have previously reported, HDM is complex mix of various proteins, which can result in relatively low concentration of protein adsorbed.¹⁴³ Additionally, a previous study observed that there were changes in corona concentration between pristine and functionalized MWCNTs due to the changes in surface charge, which would affect the electrostatic interaction between proteins and MWCNTs.^{167,168} The surface charge of between pristine and purified MWCNTs has been observed to similar, which would offer a possible explanation for the similarities in HDM adsorption between pristine, CP, and TP MWCNTs.¹⁶⁹

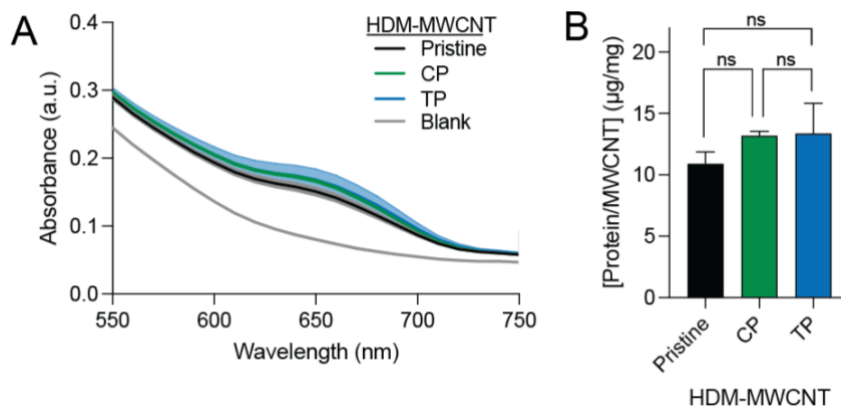


Figure 4-3: Protein concentration of the HDM corona formed on pristine, CP, and TP MWCNTs. (A) All 3 types of MWCNTs (1 mg mL^{-1}) were incubated with increasing concentrations of HDM (1 mg mL^{-1}). The concentration of the resulting corona was measured with a colorimetric protein assay (660 nm assay; $n = 3$ distinct samples). Solid lines show the mean and shading shows the standard deviation. (B) Protein concentration of the resulting corona. Significance was calculated using an ANOVA with a *post hoc* Tukey test. ns = not significant.

4.3.3 Composition of HDM coronas on pristine and purified MWCNTs

The composition of HDM (1 mg mL^{-1}) incubated with pristine, CP, and TP MWCNTs (1 mg mL^{-1}) was visually compared using gel electrophoresis (Figure 4-4). In comparison to HDM protein, all 3 HDM-MWCNT showed an increase in the band ~ 15 kDa. We previously identified a 15 kDa protein in HDM-MWCNT as Der p 2.¹⁴³ There were no notable differences between the pristine and purified MWCNTs observed on the gel. Given the similarities in composition and concentration of HDM proteins between the pristine and purified MWCNTs, it is possible that purification does not impact the interactions between HDM and MWCNTs. Moreover, the increase in the 15 kDa band suggests that purified HDM-MWCNT are dominated by Der p 2.

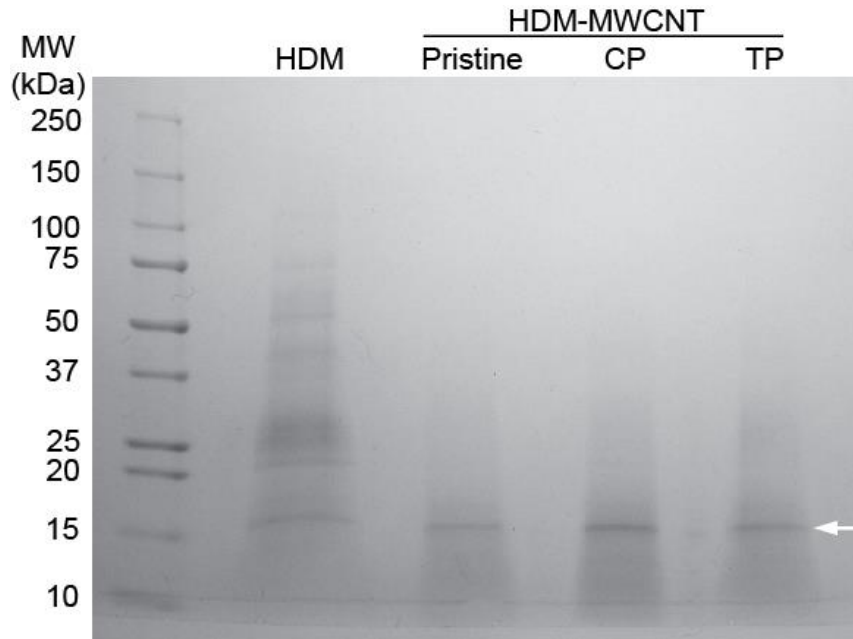


Figure 4-4: Gel electrophoresis used to compare the composition of HDM corona on pristine, CP, and TP MWCNTs. Arrow highlights the darkest band at ~15 kDa.

4.4 Conclusions

To study the effects of inhaling pristine, purified, and functionalized MWCNTs, we analyzed the concentration of BSA adsorbed to the surface of various MWCNTs. BSA was used as representative protein for lung fluid. The protein concentration of BSA-MWCNT coronas was analyzed as a function of initial protein concentration. The concentration of BSA proteins that adsorb onto the surface of pristine, purified, and functionalized MWCNTs was unique to each type of MWCNT. A linear relationship between the initial protein concentration and the concentration of protein adsorbed was found only using pristine MWCNTs. The concentration of protein adsorbed did not vary significantly when the initial concentration of protein was increased for TP and TP+COOH MWCNTs. This could have been due to the variance within sample groups.

More samples would need to be measured in order to understand if the lack of a trend is an attribute of TP and TP+COOH MWCNTs.

In addition to BSA proteins, the concentration of HDM proteins on pristine, CP, and TP MWCNTs was compared. There were no statistically significant differences between the concentration of HDM adsorbed on each type of MWCNTs. Composition of the coronas was also compared across pristine, CP, and TP MWCNT using gel electrophoresis. Although no notable differences were found, a 15 kDa band was shown in relatively high abundance in all coronas. Based on previous results, this band indicated an abundance of Der p 2 proteins in the coronas. Proteomic analysis of HDM-MWCNT, using purified and functionalized MWCNTs would provide greater insight to the effects of surface modification on the composition of MWCNT corona.

5. Indium tin oxide based nanofluid for laser lithotripsy treatment²

Laser lithotripsy, a common procedure for the treatment of kidney stones, can cause thermal damage to kidney and surrounding tissues. We present the use of nanofluid to mitigate thermal damage. The proposed nanofluid is comprised of indium tin oxide-silica nanoparticles (ITO@SiO₂ NPs). For clinical applications, the nanofluid must ensure optical visibility for endoscopic procedures and biological safety. We analyze the stability of ITO@SiO₂ NPs in solution by measuring indium and tin concentrations in supernatant samples using inductively coupled plasma mass spectrometry (ICP-MS). The presence of indium and tin ions in the supernatants would indicate NP disintegration. To evaluate the stability of ITO@SiO₂ NPs after laser exposure, ITO@SiO₂ NPs were irradiated with a Ho:YAG laser at 0.2 J/20 Hz for 1000 pulses. Concentrations of indium and tin in these samples were also measured. The results confirm that ITO@SiO₂ NPs remained stable in solution post-synthesis and after laser exposure. The cytotoxicity of bare ITO and ITO@SiO₂ NPs was tested on murine epithelial cells using an MTT assay. Cells were exposed NPs at a concentration of 0.25 wt%, selected for its optical transparency, for 1 hour or 24 hours. After 1 hour and 24 hours, cells remained healthy after exposure to both bare and silica coated ITO NPs. These studies present a

² The research in this chapter was done as a collaboration with Qingsong Fan, Junqin Chen, Judith Dominguez and Professors Christine Payne, Pei Zhong and Po-Chun Hsu.

promising a nanofluid, to be used alongside laser lithotripsy, for the treatment of kidney stones.

5.1 Introduction

Urinary stone disease (USD), also known as kidney stones, is a common disorder that approximately 13% of men and 7% of women will be diagnosed with in the United States.¹⁷⁰ Kidney stones can vary in size, shape, and chemical compositions.¹⁷¹ The most common type of stones are calcium oxalate and calcium phosphate stones.¹⁷² USD symptoms are related to the stone location, which can be located in the kidney, ureter, or urinary bladder. The main symptom is pain, which can range from mild to severe pain in areas such as the lower abdomen and back.¹⁷³ The three most common treatments for kidney stones include extracorporeal shock wave lithotripsy (ESWL), rigid or flexible ureteroscopic stone fragmentation and retrieval (URS) and percutaneous surgery.¹⁷⁴

URS is the preferred method for treating ureteral and renal stones <20 mm.^{53,175} In 1992, Ho:YAG laser lithotripsy became the ideal method for stone ablation during URS.^{56,176} The advantages of the Ho:YAG laser include: 1) ability to effectively fragment various types of stones; 2) the thin (200 μm) and flexible fibers have limited energy losses; 3) low risk of tissue damage because of the high adsorption coefficient of the laser in water; 4) can be used for soft tissue applications.^{55,177-181} Even though Ho:YAG laser lithotripsy is an effective treatment for kidney stones, there are concerns are still concern

regarding thermal damage. Previous studies have reported significant temperature increases in the kidney conduits, through which urine passes.^{182–184}

In this study, we integrate a ITO@SiO₂ nanofluid to Ho:YAG laser lithotripsy to reduce temperature increases that could damage surrounding tissues. ITO nanoparticles have a high optical transmission (>80%) in the visible region.^{185,186} This makes an ITO nanofluid ideal for URS because it offers a minimal obstructed view during the procedure. ITO is also known to have a high thermal tolerance, which would allow the nanofluid to withstand the temperatures of Ho:YAG laser pulses. The experiments presented aim to test the stability of ITO@SiO₂ in solution and after laser exposure. We also test the cytotoxicity of bare and ITO@SiO₂.

5.2 Materials and Methods

5.2.1 Inductively coupled plasma mass spectrometry (ICP-MS)

ITO@SiO₂ nanoparticles were synthesized by the Hsu Group at the University of Chicago. To measure concentrations of indium and tin in ITO@SiO₂ supernatants, centrifugation or dialysis were used to separate NPs and supernatants. ITO@SiO₂ (1 wt%) samples were washed by centrifugation (15 min, 4 °C, 14 000 rpm) 3x. After each wash, the supernatant was collected filtered using 10 kDa spin columns with 10kDa pores (#431478, Corning, Corning, NY) to remove remaining NPs in the solution. Dialysis was also used to separate nanoparticles from the supernatant by loading ITO@SiO₂ (1 wt%) to a 100 kDa dialysis device with a 100 kDa pore membrane (#G235035, Repligen, Rancho Dominguez, Ca). The dialysis device was prepared using

manufacturer specification. The sample was dialyzed at RT for 12 hours, and the supernatant was collected.

Residual indium and tin concentrations were also measured after ITO@SiO₂ were irradiated using a holmium (Ho):YAG laser (0.2 J/20 Hz, 1000 pulses). Samples were centrifuged (15 min, 4 °C, 14 000 rpm), and supernatants were collected. The concentrations of indium and tin in irradiated supernatant samples were compared against irradiated nanoparticle samples and non-irradiated supernatants. ICP-MS (7900; Agilent) was used to measure indium and tin concentrations in all samples.

5.2.2 Cell culture

A murine epithelial cell line (mIMCD-3, ATCC, Manassas, VA) was used for all experiments. Cells were cultured in Dulbecco's Modified Eagle Medium/Hams F-12 (DMEM/F-12; pH 7.4, #11320033, Thermo Fisher, Waltham, MA), supplemented with 10 % fetal bovine serum (FBS, #10437028, Thermo Fisher). Cells were grown at 5% CO₂ at 37 °C and passaged upon reaching 80% confluency with a maximum passage number of 20.

5.2.3 MTT assay

MIMCD-3 cells were seeded onto sterile 24-well plates (#3524, Corning Inc, Corning NY) at a density of 150,000 cells per well. The cells were cultured overnight and incubated with ITO@SiO₂ (0.25 wt.%) for 1 h or 24 h. Control cells were incubated in DMEM/F-12 media for the duration of the treatment. Incubation with Triton X-100 (10% in Dulbecco's Phosphate Buffered Saline (PBS), 30 s exposure; X100-100ML, Millipore

Sigma, Burlington, MA) was used to damage cells, serving as a positive control. Cells were washed 3 times in PBS (pH 7.3-7.5, #28374, Thermo Fisher). Cells were incubated in DMEM (300 μ l; #31053028, Thermo Fisher) and 3-(4,5-dimethylthiazol-2-yl)-2,5-diphenyl tetrazolium bromide (MTT, 0.5 mg ml⁻¹, #V13154, Thermo Fisher) for 1 h. Media was aspirated, and cells were incubated in dimethyl sulfoxide (300 μ l; DMSO, #D8418, Millipore Sigma) for 10 minutes in the dark. DMSO was transferred into a clear 96-well plate (#82050, VWR, Radnor, PA) and absorbance was measured at 580 nm using a plate reader (SpectraMax iD3, Molecular Devices, San Jose, CA).

5.3 Results and Discussion

5.3.1 ITO@SiO₂ nanoparticles are stable in solution

ITO@SiO₂ nanoparticles were suspended in water after synthesis. The ITO@SiO₂ NPs were created ensuring colloidal stability. To investigate if the NPs were deteriorating while in solutions, we measured the concentrations of indium and tin present in supernatant samples. Supernatants were collected using two methods: centrifugation (Figure 5-1A) and dialysis (Figure 5-1B). ICP-MS was used to measure the concentrations of indium and tin in each sample.

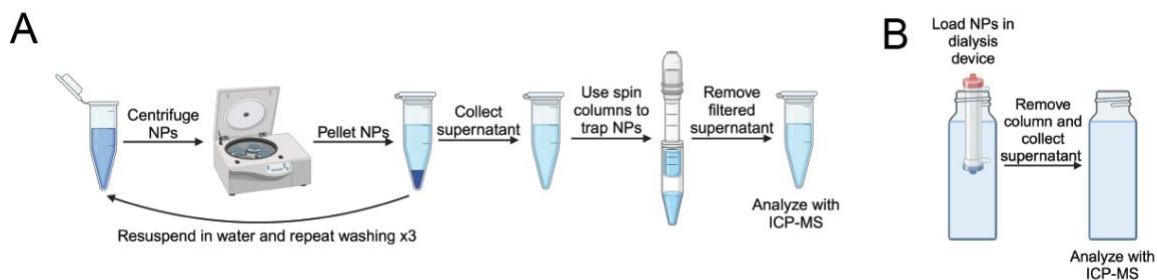


Figure 5-1: Measuring indium and tin in ITO@SiO₂ supernatant. Methods used included (A) washing nanoparticles by centrifugation x3 and (B) by using a dialysis device.

Low concentrations of indium (12.0 µg/L) and tin (1.94 µg/L) were found in the first filtered wash (Table 5-1: Indium and tin concentrations in each sample collected by separating the nanoparticles from the supernatant using centrifugation and a dialysis device.. The second and third washes that followed contained concentrations that were below the limit of detection of the instrument. From this, we can infer that the first filtered wash contained nanoparticles that were able to permeate the spin column membrane. The remaining nanoparticles were caught by spin columns used to filter the second and the third wash. Indium and tin were also not detected in the supernatant collected using dialysis (Table 5-1). The undetectable concentrations of indium and tin confirm ITO@SiO₂ nanoparticles do not dissolve in water after synthesis.

Table 5-1: Indium and tin concentrations in each sample collected by separating the nanoparticles from the supernatant using centrifugation and a dialysis device.

| | | [Indium] (µg/L) | [Tin] (µg/L) |
|---------------------|-----------------------------|-----------------|--------------|
| | Filtered wash 1 | 12.0 | 1.94 |
| Centrifuging | Filtered wash 2 | <1.00 | <1.00 |
| | Filtered wash 3 | <1.00 | <1.00 |
| | Dialysis Supernatant | <1.00 | <1.00 |

5.3.2 Indium and tin are not released from ITO@SiO₂ nanoparticles following irradiation

The laser lithotripsy procedure will require the ITO@SiO₂ to withstand the energy and frequency needed to fragment kidney stones. The structure of the ITO@SiO₂ nanoparticles must be retained to avoid the release of indium and tin into the kidneys. We investigated the effects of laser exposure by irradiating 1 wt% of ITO with a Ho:YAG laser at 0.2 J/20 Hz for 1000 pulses. After irradiation, the composition of the nanoparticles and the supernatant were analyzed using ICP-MS (Figure 5-2). The supernatant was collected by centrifuging the irradiated to separate the nanoparticles from the suspension solution. Concentrations of indium and tin were compared against the supernatant of a non-irradiated sample, as a control. Additionally, the concentration of indium and tin in a sample of an irradiated ITO@SiO₂ nanoparticles was measured to contextualize the concentrations in the supernatants.

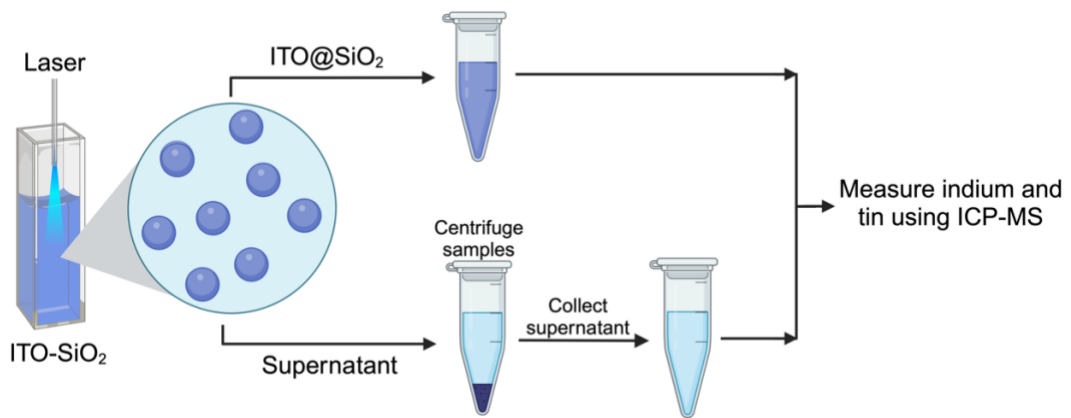


Figure 5-2: Schematic of collecting supernatant and ITO@SiO₂ following irradiation.

Indium and tin concentrations in supernatant from irradiated samples were similar to the concentrations in the control supernatant (Table 5-2). The concentration of tin in the supernatant of irradiated samples was $3.0 \pm 0.1 \text{ mg L}^{-1}$ compared to $3.6 \pm 0.1 \text{ mg L}^{-1}$ in the control supernatant. Likewise, the concentration of indium between irradiated ($38.1 \pm 1.9 \text{ mg L}^{-1}$) and control ($39.1 \pm 2.0 \text{ mg L}^{-1}$) supernatants are comparable. Furthermore, the concentrations of indium and tin in the irradiated supernatant are over 100x lower than the concentrations measured in the irradiated nanoparticles. This demonstrates that the concentrations of indium and tin measured in the irradiated NP samples were from intact ITO@SiO₂ NPs, rather than the decomposition of the NPs into indium and tin (elemental) fragments. The presence of both elements in the control and irradiated supernatants indicated that there was likely trace amounts ITO@SiO₂ NPs that were unable to remain a part of pellet formed by centrifugation. Because there is no filtering process following the introduction of the sample into the ICP-MS instrument, the instrument measured the concentration of indium and tin in the trace amounts of ITO@SiO₂ NPs, rather than any decomposition of the NPs. It is important to understand the dissolution behavior of this nanofluid, especially in the context of laser interactions. Decomposition of the NPs can affect the toxicity of the fluid to surrounding tissues. Therefore, investigating the composition of ITO@SiO₂ following irradiation will allow us to understand the biological effects of using this nanofluid during laser lithotripsy.

Table 5-2: Concentration of indium and tin in supernatant and NPs following irradiation. A Ho:YAG laser was used at 0.2 J/20 Hz for 1000 pulses. Irradiated samples were compared to a control supernatant (n=2 for each condition).

| | Control | Irradiated | |
|----------------------|----------------|-------------------|---------------|
| | Supernatant | Supernatant | Nanoparticles |
| Tin (mg/L) | 3.6 ± 0.1 | 3.0 ± 0.1 | 326.3 ± 0.9 |
| Indium (mg/L) | 39.1 ± 2.0 | 38.1 ± 1.9 | 6279.6 ± 7.6 |

5.3.3 Cells health is maintained following exposure to bare ITO nanoparticles

The toxicity of ITO NPs without a silicon dioxide (SiO₂) coating (bare ITO) must be investigated before the application of ITO@SiO₂ in clinical practices. The ITO NPs used designed for laser lithotripsy treatment will have a SiO₂ coating. In the case, that the thickness of coating is becomes inconsistent during the synthesis process or that the coating is damaged during the treatment, we need to analyze the biological effects of bare ITO NP exposure. We incubated murine epithelial cells with a 0.25 wt% bare ITO solution for 1 hour and 24 hours. The cell viability results from the experiment are summarized in Figure 5-3. Should the SiO₂ coating on the ITO@SiO₂ NPs become damaged, the bare ITO NPs demonstrate a non-significant amount of toxicity to human kidney tissues.

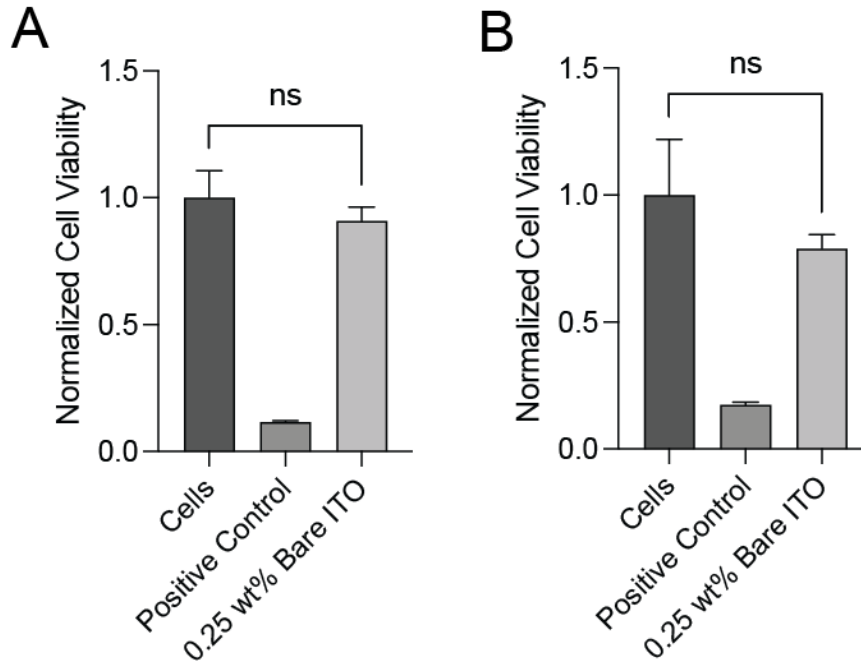


Figure 5-3: Viability of mIMCD-3 cells, measured with a MTT assay, after incubation with 0.25 wt% bare ITO. Exposure to triton X-100 (10% in PBS, 30 s) was used as a positive control to decrease cell viability. (A) 1 h incubation. (B) 24 h incubation. Significance was measured using a 1-way ANOVA with Dunnett's multiple comparisons post hoc. ns – not significant.

5.3.4 Cells remain healthy after interactions with ITO@SiO₂ NPs

The nanoparticles intended to be utilized during laser lithotripsy treatments are ITO@SiO₂. In order for these particles to be used during treatments, the nanofluid must allow for physician to maintain optical view of the kidney cavity with an endoscope and it must be biologically safe. Optical transparency was achieved at concentrations of 0.25 wt% and lower. Biocompatibility was addressed by the addition of a SiO₂ coating on the ITO NPs. We tested the viability of murine epithelial (mIMCD-3) cells 0.25 wt% ITO@SiO₂ after a 1-hour and a 24-hour incubation. The duration for laser lithotripsy procedures will typically not exceed 1 hour. Therefore, testing a 24-hour incubation

serves as a benchmark for an extreme condition. The results demonstrated that the cell viability was not significantly affected by 1-hour or 24-hour interactions with 0.25 wt% ITO@SiO₂ (Figure 5-4). Given the duration of laser lithotripsy and the moderate concentration, the use of ITO@SiO₂ suggests limited toxicity to kidney tissues.

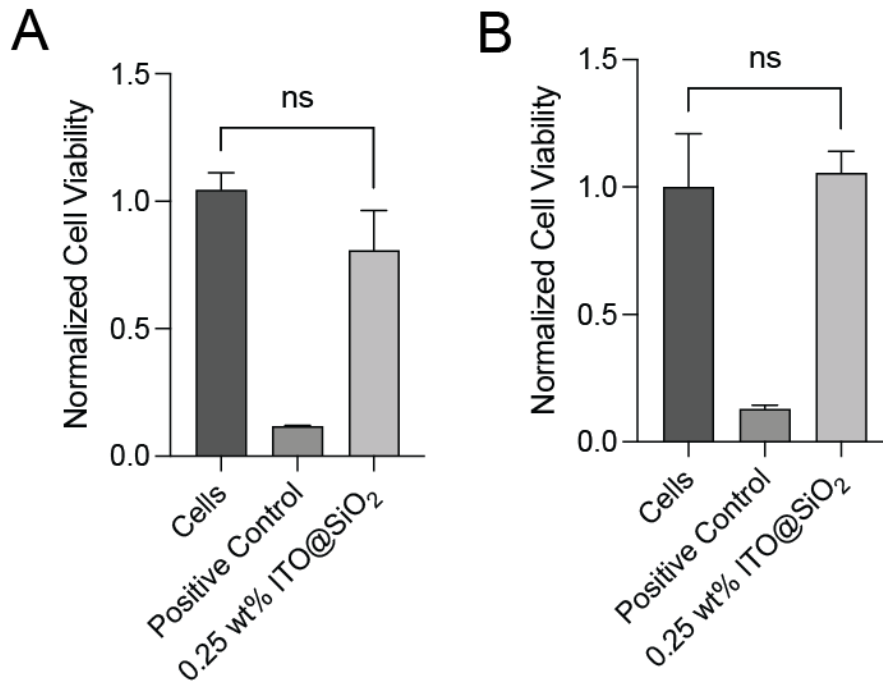


Figure 5-4: Viability of mIMCD-3 cells, measured with a MTT assay, after incubation with 0.25 wt% ITO@SiO₂. Exposure to triton X-100 (10% in PBS, 30 s) was used as a positive control to decrease cell viability. (A) 1 h incubation. (B) 24 h incubation. Significance was measured using a 1-way ANOVA with Dunnett's multiple comparisons post hoc. ns – not significant.

5.4 Conclusions

The nanofluid designed to reduce thermal damage to tissues surrounding the kidneys during laser lithotripsy treatments consists of ITO@SiO₂ NPs. To determine the stability of the ITO@SiO₂ NPs in solution, we measured the concentrations of indium

and tin in the supernatant samples. The absence of detectable indium and tin concentrations in the supernatant confirms that ITO@SiO₂ NPs remain stable and do not dissolve in water after synthesis. The stability of ITO@SiO₂ nanoparticles was investigated after laser exposure by irradiating 1 wt% of ITO@SiO₂ nanoparticles with a Ho:YAG laser at 0.2 J/20 Hz for 1000 pulses. Results showed that the structure ITO@SiO₂ NPs were unharmed after laser exposure.

We also tested the cytotoxicity of bare ITO and ITO@SiO₂ nanoparticles on murine epithelial cells. If the SiO₂ coating on the ITO@SiO₂ nanoparticles is damaged, the exposed ITO NPs exhibit minimal toxicity to human kidney tissues. A concentration of 0.25 wt% was used for cytotoxicity test because of the optical transparency of this concentration. For the nanofluid to be effective during laser lithotripsy, the nanofluid must enable the physician to maintain an optical view of the kidney cavity using an endoscope, while also ensuring biological safety. The results for both bare and silica coated ITO NPs revealed minimal cell toxicity at 0.25 wt%. Future experiments should focus on examining the possibility of internalization of ITO@SiO₂ by cells, characterizing the interactions of ITO@SiO₂ with synthetic urine, and measuring the cytotoxicity of ITO@SiO₂ at increasing concentrations.

6. Conclusion

6.1 Summary Work

One goal of this work was to model real-world exposure to MWCNTs by examining the interaction between HDM proteins and MWCNTs. Using a combination of XPS, gel electrophoresis, protein concentration assays, western blotting, and proteomics, we observed that HDM proteins adsorb onto the surface of MWCNTs, forming a protein corona. The protein corona formed will dictate the biological response to nanomaterials. We hypothesize that the HDM corona will influence the cellular and in vivo response to HDM–MWCNT interactions. Our findings show that Der p 2, a major HDM allergen, becomes highly concentrated on the MWCNT surface. Der p 2 remains abundant even after HDM-MWCNT interact with BALF or BSA, a representing lung fluid protein. This suggests that lung fluid is unlikely to mitigate the physiological response triggered by the high concentration of Der p 2.

We aimed to understand the allergic potential of the Der p 2 abundant HDM corona by analyzing the enzyme activity of interactions between HDM and MWCNTs. HDM contains cysteine and serine proteases, enzymes that break down protein, that contribute to the pathophysiology of allergic airway diseases when active. To quantify the activity of these proteases, we measured the enzyme concentration of HDM free in solution, HDM mixed with MWCNTs, and HDM adsorbed on to the surface of MWCNTs. The results from this comparison showed that HDM-MWCNT contained the lowest concentration of active enzymes, which could suggest that HDM adsorbed on to

MWCNTs will not exacerbate allergic airway diseases. Isolated cysteine and serine protease interactions with MWCNTs and PS NPs were also investigated by comparing the active concentration enzyme concentration of free enzymes against the active enzyme concentration of the proteases adsorbed onto each nanomaterial. Free enzymes contained a higher concentration of active compared to enzyme coronas. Lack of high enzyme activity in both enzyme-MWCNT and enzyme-PS coronas suggests the structure of papain and trypsin proteases contributed to loss of enzyme activity along with the electrostatic interactions between the enzymes and nanomaterials.

To study the effects of inhaling MWCNTs, we analyzed the concentration of albumin adsorbed to pristine, purified, and functionalized MWCNTs. The protein concentration albumin coronas were analyzed as a function of initial protein concentration. The concentration of albumin proteins on the surface of pristine, purified, and functionalized MWCNTs was unique to each type of MWCNT. In addition of BSA proteins, the concentration of HDM proteins on pristine, CP, and TP MWCNTs was compared. There were no statically significant differences between the concentration of HDM adsorbed on to each type of MWCNTs. Composition of the coronas was also compared across pristine, CP, and TP MWCNT using gel electrophoresis. Although no notable differences were found, a 15 kDa band, likely Der p 2, was shown in relatively high abundance in all coronas.

A final aim of this work was to demonstrate the potential nanomaterials have toward advancing medical treatments. We characterized indium tin oxide nanoparticles

coated with silica dioxide (ITO@SiO₂ nanofluid) to reduce thermal damage during kidney stone laser lithotripsy. Stability tests showed no evidence of nanoparticle disintegration in solution or under extreme laser exposure. Cytotoxicity testing at 0.25 wt% indicated low risks to cell viability. These findings suggest MWCNT interactions with lung proteins and allergens are complex, and that ITO@SiO₂ nanofluid is promising for lithotripsy, demonstrating the versatile applications and relative safety of nanomaterials.

6.2 Future Work

Future work will extend to analyzing allergen adsorption on MWCNTs following common purification methods and chemical functionalizations to determine if these results are general. Proteomic analysis of HDM-MWCNT, using purified and functionalized MWCNTs would provide greater insight to the effects of surface modification on the composition of MWCNT corona. Experiments should also focus on examining the possible of internalization of ITO@SiO₂ by cells, characterizing the interactions of ITO@SiO₂ with synthetic urine, and measuring the cytotoxicity of ITO@SiO₂ at increasing concentrations.

7. References

1. Wu, C. *et al.* Nano Materials and its Application in Space. *AMM* **482**, 34–37 (2013).
2. Kučuk, N., Primožič, M., Knez, Ž. & Leitgeb, M. Sustainable Biodegradable Biopolymer-Based Nanoparticles for Healthcare Applications. *IJMS* **24**, 3188 (2023).
3. Kolahalam, L. A. *et al.* Review on nanomaterials: Synthesis and applications. *Materials Today: Proceedings* **18**, 2182–2190 (2019).
4. Joudeh, N. & Linke, D. Nanoparticle classification, physicochemical properties, characterization, and applications: a comprehensive review for biologists. *J Nanobiotechnol* **20**, 262 (2022).
5. Wu, Q., Miao, W., Zhang, Y., Gao, H. & Hui, D. Mechanical properties of nanomaterials: A review. *Nanotechnology Reviews* **9**, 259–273 (2020).
6. *The Global Market for Nanomaterials 2021-2031: Markets, Applications, Productions, and Producers.* (2021).
7. *Nanostructured Materials for Engineering Applications.* (Springer Berlin Heidelberg, Berlin, Heidelberg, 2011). doi:10.1007/978-3-642-19131-2.
8. Brock, S. L. Nanostructures and Nanomaterials: Synthesis, Properties and Applications By Guozhang Cao (University of Washington). Imperial College Press (distributed by World Scientific): London. 2004. xiv + 434 pp. \$78.00. ISBN 1-86094-415-9. *J. Am. Chem. Soc.* **126**, 14679–14679 (2004).
9. Catita, J. A. M. Challenges in Nanomaterial Characterization – From Definition to Analysis. in *Nanotoxicology in Safety Assessment of Nanomaterials* (eds. Louro, H. & Silva, M. J.) vol. 1357 3–17 (Springer International Publishing, Cham, 2022).
10. Oberdörster, G. *et al.* Translocation of Inhaled Ultrafine Particles to the Brain. *Inhalation Toxicology* **16**, 437–445 (2004).
11. Ray, P. C., Yu, H. & Fu, P. P. Toxicity and Environmental Risks of Nanomaterials: Challenges and Future Needs. *Journal of Environmental Science and Health, Part C* **27**, 1–35 (2009).
12. Oberdörster, G. *et al.* EXTRAPULMONARY TRANSLOCATION OF ULTRAFINE CARBON PARTICLES FOLLOWING WHOLE-BODY INHALATION EXPOSURE OF RATS. *Journal of Toxicology and Environmental Health, Part A* **65**, 1531–1543 (2002).

13. Hillaireau, H. & Couvreur, P. Nanocarriers' entry into the cell: relevance to drug delivery. *Cell. Mol. Life Sci.* **66**, 2873–2896 (2009).
14. Dawson, K. A., Salvati, A. & Lynch, I. Nanoparticles reconstruct lipids. *Nature Nanotech* **4**, 84–85 (2009).
15. Capco, D. G. & Chen, Y. *Nanomaterial: Impacts on Cell Biology and Medicine*. (Springer, Dordrecht, 2014).
16. Street, R. A. Thin-Film Transistors. *Advanced Materials* **21**, 2007–2022 (2009).
17. Franklin, A. D. Nanomaterials in transistors: From high-performance to thin-film applications. *Science* **349**, aab2750 (2015).
18. Francis, A. P. & Devasena, T. Toxicity of carbon nanotubes: A review. *Toxicol Ind Health* **34**, 200–210 (2018).
19. Yang, K., Li, Y., Tan, X., Peng, R. & Liu, Z. Behavior and Toxicity of Graphene and Its Functionalized Derivatives in Biological Systems. *Small* **9**, 1492–1503 (2013).
20. Devasena, T., Francis, A. P. & Ramaprabhu, S. Toxicity of Graphene: An Update. in *Reviews of Environmental Contamination and Toxicology Volume 259* (ed. De Voogt, P.) vol. 259 51–76 (Springer International Publishing, Cham, 2021).
21. Ou, L. *et al.* Toxicity of graphene-family nanoparticles: a general review of the origins and mechanisms. *Part Fibre Toxicol* **13**, 57 (2016).
22. Singh, S. P. *et al.* Toxicity assessment of manganese oxide micro and nanoparticles in Wistar rats after 28 days of repeated oral exposure. *J of Applied Toxicology* **33**, 1165–1179 (2013).
23. Crossgrove, J. & Zheng, W. Manganese toxicity upon overexposure. *NMR in Biomedicine* **17**, 544–553 (2004).
24. Landsiedel, R. *et al.* Inhalation studies for the safety assessment of nanomaterials: status quo and the way forward. *WIREs Nanomed Nanobiotechnol* **4**, 399–413 (2012).
25. Klein, C. L. *et al.* Hazard identification of inhaled nanomaterials: making use of short-term inhalation studies. *Arch Toxicol* **86**, 1137–1151 (2012).
26. *Nanotechnology - Toxicological Issues and Environmental Safety: Proceedings of the Nato Advanced Research Workshop on Nanotechnology - Toxicological Issues and Environmental Safety, Varna, Bulgaria, 12 - 17 August 2006*. (Springer Netherlands, Dordrecht, 2007). doi:10.1007/978-1-4020-6076-2.

27. Shvedova, A. A. *et al.* Inhalation vs. aspiration of single-walled carbon nanotubes in C57BL/6 mice: inflammation, fibrosis, oxidative stress, and mutagenesis. *American Journal of Physiology-Lung Cellular and Molecular Physiology* **295**, L552–L565 (2008).
28. Oberdörster, G., Castranova, V., Asgharian, B. & Sayre, P. Inhalation Exposure to Carbon Nanotubes (CNT) and Carbon Nanofibers (CNF): Methodology and Dosimetry. *Journal of Toxicology and Environmental Health, Part B* **18**, 121–212 (2015).
29. Ma-Hock, L. *et al.* Inhalation Toxicity of Multiwall Carbon Nanotubes in Rats Exposed for 3 Months. *Toxicological Sciences* **112**, 468–481 (2009).
30. Kinaret, P. *et al.* Inhalation and Oropharyngeal Aspiration Exposure to Rod-Like Carbon Nanotubes Induce Similar Airway Inflammation and Biological Responses in Mouse Lungs. *ACS Nano* **11**, 291–303 (2017).
31. Mercer, R. R. *et al.* Distribution and fibrotic response following inhalation exposure to multi-walled carbon nanotubes. *Part Fibre Toxicol* **10**, 33 (2013).
32. Bottini, M. *et al.* Multi-walled carbon nanotubes induce T lymphocyte apoptosis. *Toxicology Letters* **160**, 121–126 (2006).
33. Erdely, A. *et al.* Carbon nanotube dosimetry: from workplace exposure assessment to inhalation toxicology. *Part Fibre Toxicol* **10**, 53 (2013).
34. Morimoto, Y., Horie, M., Kobayashi, N., Shinohara, N. & Shimada, M. Inhalation Toxicity Assessment of Carbon-Based Nanoparticles. *Acc. Chem. Res.* **46**, 770–781 (2013).
35. Saptarshi, S. R., Duschl, A. & Lopata, A. L. Interaction of nanoparticles with proteins: relation to bio-reactivity of the nanoparticle. *J Nanobiotechnol* **11**, 26 (2013).
36. Lynch, I. & Dawson, K. A. Protein-nanoparticle interactions. *Nano Today* **3**, 40–47 (2008).
37. Kukovecz, Á., Kozma, G. & Kónya, Z. Multi-Walled Carbon Nanotubes. in *Springer Handbook of Nanomaterials* (ed. Vajtai, R.) 147–188 (Springer Berlin Heidelberg, Berlin, Heidelberg, 2013). doi:10.1007/978-3-642-20595-8_5.
38. Iijima, S. & Ichihashi, T. Single-shell carbon nanotubes of 1-nm diameter. *Nature* **363**, 603–605 (1993).
39. Ajayan, P. M. Nanotubes from Carbon. *Chem. Rev.* **99**, 1787–1800 (1999).

40. Chen, Z. *et al.* Opportunities for graphene, single-walled and multi-walled carbon nanotube applications in agriculture: A review. *Crop Design* **1**, 100006 (2022).
41. Kukovecz, Á., Kozma, G. & Kónya, Z. Multi-Walled Carbon Nanotubes. in *Springer Handbook of Nanomaterials* (ed. Vajtai, R.) 147–188 (Springer Berlin Heidelberg, Berlin, Heidelberg, 2013). doi:10.1007/978-3-642-20595-8_5.
42. Stoner, B. R., Brown, B. & Glass, J. T. Selected topics on the synthesis, properties and applications of multiwalled carbon nanotubes. *Diamond and Related Materials* **42**, 49–57 (2014).
43. Frank, S., Poncharal, P., Wang, Z. L. & Heer, W. A. D. Carbon Nanotube Quantum Resistors. *Science* **280**, 1744–1746 (1998).
44. Wong, E. W., Sheehan, P. E. & Lieber, C. M. Nanobeam Mechanics: Elasticity, Strength, and Toughness of Nanorods and Nanotubes. *Science* **277**, 1971–1975 (1997).
45. Taylor-Just, A. J. *et al.* The pulmonary toxicity of carboxylated or aminated multi-walled carbon nanotubes in mice is determined by the prior purification method. *Part Fibre Toxicol* **17**, 60 (2020).
46. Duke, K. S. & Bonner, J. C. Mechanisms of carbon nanotube-induced pulmonary fibrosis: a physicochemical characteristic perspective. *WIREs Nanomed Nanobiotechnol* **10**, e1498 (2018).
47. Payne, C. K. A protein corona primer for physical chemists. *The Journal of Chemical Physics* **151**, 130901 (2019).
48. Docter, D. *et al.* No King without A Crown – Impact of the Nanomaterial-Protein Corona on Nanobiomedicine. *Nanomedicine (Lond.)* **10**, 503–519 (2015).
49. Khan, S. R. *et al.* Correction: Kidney stones. *Nat Rev Dis Primers* **3**, 17001 (2017).
50. Pearle, M. S. *et al.* PROSPECTIVE, RANDOMIZED TRIAL COMPARING SHOCK WAVE LITHOTRIPSY AND URETEROSCOPY FOR LOWER POLE CALICEAL CALCULI 1 CM OR LESS. *Journal of Urology* **173**, 2005–2009 (2005).
51. Albala, D. M. *et al.* LOWER POLE I: A PROSPECTIVE RANDOMIZED TRIAL OF EXTRACORPOREAL SHOCK WAVE LITHOTRIPSY AND PERCUTANEOUS NEPHROSTOLITHOTOMY FOR LOWER POLE NEPHROLITHIASIS—INITIAL RESULTS. *Journal of Urology* **166**, 2072–2080 (2001).

52. Scales, C. D. *et al.* Comparative Effectiveness of Shock Wave Lithotripsy and Ureterscopy for Treating Patients With Kidney Stones. *JAMA Surg* **149**, 648 (2014).
53. Dretler, S. P. Laser lithotripsy: A review of 20 years of research and clinical applications. *Lasers Surg Med* **8**, 341–356 (1988).
54. Wignall, G. R., Canales, B. K., Denstedt, J. D. & Monga, M. Minimally Invasive Approaches to Upper Urinary Tract Urolithiasis. *Urologic Clinics of North America* **35**, 441–454 (2008).
55. Teichman, J. M. H., Vassar, G. J., Bishoff, J. T. & Bellman, G. C. HOLMIUM: YAG LITHOTRIPSY YIELDS SMALLER FRAGMENTS THAN LITHOCLAST, PULSED DYE LASER OR ELECTROHYDRAULIC LITHOTRIPSY. *Journal of Urology* **159**, 17–23 (1998).
56. Johnson, D. E., Cromeens, D. M. & Price, R. E. Use of the holmium:YAG laser in urology. *Lasers Surg Med* **12**, 353–363 (1992).
57. Ganpule, A. P., Vijayakumar, M., Malpani, A. & Desai, M. R. Percutaneous nephrolithotomy (PCNL) a critical review. *International Journal of Surgery* **36**, 660–664 (2016).
58. Rathod, V. T., Kumar, J. S. & Jain, A. Polymer and ceramic nanocomposites for aerospace applications. *Appl Nanosci* **7**, 519–548 (2017).
59. *Carbon Nanotubes Market Size, Share & Trends Analysis Report By Product (SWNT, MWNT), By Application (Polymers, Energy, Electrical & Electronics), And Segment Forecasts, 2015 - 2022.* (2022).
60. Donaldson, K. *et al.* Carbon Nanotubes: A Review of Their Properties in Relation to Pulmonary Toxicology and Workplace Safety. *Toxicological Sciences* **92**, 5–22 (2006).
61. Ryman-Rasmussen, J. P. *et al.* Inhaled carbon nanotubes reach the subpleural tissue in mice. *Nature Nanotech* **4**, 747–751 (2009).
62. Guseva Canu, I., Batsungnoen, K., Maynard, A. & Hopf, N. B. State of knowledge on the occupational exposure to carbon nanotubes. *International Journal of Hygiene and Environmental Health* **225**, 113472 (2020).
63. Wright, M. D., Buckley, A. J. & Smith, R. Estimates of carbon nanotube deposition in the lung: improving quality and robustness. *Inhalation Toxicology* **32**, 282–298 (2020).

64. Muller, J. *et al.* Respiratory toxicity of multi-wall carbon nanotubes. *Toxicology and Applied Pharmacology* **207**, 221–231 (2005).
65. Porter, D. W. *et al.* Mouse pulmonary dose- and time course-responses induced by exposure to multi-walled carbon nanotubes. *Toxicology* **269**, 136–147 (2010).
66. Cesta, M. F. *et al.* Bacterial Lipopolysaccharide Enhances PDGF Signaling and Pulmonary Fibrosis in Rats Exposed to Carbon Nanotubes. *Am J Respir Cell Mol Biol* **43**, 142–151 (2010).
67. Ryman-Rasmussen, J. P. *et al.* Inhaled Multiwalled Carbon Nanotubes Potentiate Airway Fibrosis in Murine Allergic Asthma. *Am J Respir Cell Mol Biol* **40**, 349–358 (2009).
68. Inoue, K. *et al.* Effects of multi-walled carbon nanotubes on a murine allergic airway inflammation model. *Toxicology and Applied Pharmacology* **237**, 306–316 (2009).
69. Rydman, E. M. *et al.* Inhalation of rod-like carbon nanotubes causes unconventional allergic airway inflammation. *Part Fibre Toxicol* **11**, 48 (2014).
70. Han, S. G., Andrews, R. & Gairola, C. G. Acute pulmonary response of mice to multi-wall carbon nanotubes. *Inhalation Toxicology* **22**, 340–347 (2010).
71. Duke, K. S. *et al.* STAT1-dependent and -independent pulmonary allergic and fibrogenic responses in mice after exposure to tangled versus rod-like multi-walled carbon nanotubes. *Part Fibre Toxicol* **14**, 26 (2017).
72. *OSHA Fact Sheet: Working Safely with Nanomaterials.*
73. Lee, H. Y. *et al.* Role of the protease-activated receptor-2 (PAR2) in the exacerbation of house dust mite-induced murine allergic lung disease by multi-walled carbon nanotubes. *Part Fibre Toxicol* **20**, 32 (2023).
74. Kuempel, E. D. *et al.* Evaluating the mechanistic evidence and key data gaps in assessing the potential carcinogenicity of carbon nanotubes and nanofibers in humans. *Critical Reviews in Toxicology* **47**, 1–58 (2017).
75. Singh, A. V. *et al.* Review of emerging concepts in nanotoxicology: opportunities and challenges for safer nanomaterial design. *Toxicology Mechanisms and Methods* **29**, 378–387 (2019).
76. Nicoletti, M., Capodanno, C., Gambarotti, C. & Fasoli, E. Proteomic investigation on bio-corona of functionalized multi-walled carbon nanotubes. *Biochimica et Biophysica Acta (BBA) - General Subjects* **1862**, 2293–2303 (2018).

77. García-Hevia, L. *et al.* The unpredictable carbon nanotube biocorona and a functionalization method to prevent protein biofouling. *J Nanobiotechnol* **19**, 129 (2021).
78. Cai, X. *et al.* Characterization of carbon nanotube protein corona by using quantitative proteomics. *Nanomedicine: Nanotechnology, Biology and Medicine* **9**, 583–593 (2013).
79. Bhattacharya, K. *et al.* Biological interactions of carbon-based nanomaterials: From coronation to degradation. *Nanomedicine: Nanotechnology, Biology and Medicine* **12**, 333–351 (2016).
80. Fleischer, C. C. & Payne, C. K. Nanoparticle–Cell Interactions: Molecular Structure of the Protein Corona and Cellular Outcomes. *Acc. Chem. Res.* **47**, 2651–2659 (2014).
81. Walkey, C. D. & Chan, W. C. W. Understanding and controlling the interaction of nanomaterials with proteins in a physiological environment. *Chem. Soc. Rev.* **41**, 2780–2799 (2012).
82. Monopoli, M. P., Åberg, C., Salvati, A. & Dawson, K. A. Biomolecular coronas provide the biological identity of nanosized materials. *Nature Nanotech* **7**, 779–786 (2012).
83. Nienhaus, K. & Nienhaus, G. U. Towards a molecular-level understanding of the protein corona around nanoparticles – Recent advances and persisting challenges. *Current Opinion in Biomedical Engineering* **10**, 11–22 (2019).
84. Kobos, L. & Shannahan, J. Biocorona-induced modifications in engineered nanomaterial–cellular interactions impacting biomedical applications. *WIREs Nanomed Nanobiotechnol* **12**, e1608 (2020).
85. Ke, P. C., Lin, S., Parak, W. J., Davis, T. P. & Caruso, F. A Decade of the Protein Corona. *ACS Nano* **11**, 11773–11776 (2017).
86. Whitwell, H. *et al.* Nanoparticles in the lung and their protein corona: the few proteins that count. *Nanotoxicology* **10**, 1385–1394 (2016).
87. Poulsen, K. M., Albright, M. C., Niemuth, N. J., Tighe, R. M. & Payne, C. K. Interaction of TiO₂ nanoparticles with lung fluid proteins and the resulting macrophage inflammatory response. *Environ. Sci.: Nano* **10**, 2427–2436 (2023).
88. Thomas, W. R., Hales, B. J. & Smith, W.-A. House dust mite allergens in asthma and allergy. *Trends in Molecular Medicine* **16**, 321–328 (2010).

89. Jacquet, A. The role of innate immunity activation in house dust mite allergy. *Trends in Molecular Medicine* **17**, 604–611 (2011).
90. Calderón, M. A. *et al.* Respiratory allergy caused by house dust mites: What do we really know? *Journal of Allergy and Clinical Immunology* **136**, 38–48 (2015).
91. Plattsmills, T. *et al.* Dust mite allergens and asthma—A worldwide problem. *Journal of Allergy and Clinical Immunology* **83**, 416–427 (1989).
92. Thomas, W. R., Smith, W.-A., Hales, B. J., Mills, K. L. & O'Brien, R. M. Characterization and Immunobiology of House Dust Mite Allergens. *Int Arch Allergy Immunol* **129**, 1–18 (2002).
93. Chapman, M. D. & Platts-Mills, T. A. Purification and characterization of the major allergen from *Dermatophagoides pteronyssinus*-antigen P1. *The Journal of Immunology* **125**, 587–592 (1980).
94. Waldron, R. *et al.* Proteome and allergenome of the European house dust mite *Dermatophagoides pteronyssinus*. *PLoS ONE* **14**, e0216171 (2019).
95. Bordas-Le Floch, V. *et al.* A combined transcriptome and proteome analysis extends the allergome of house dust mite *Dermatophagoides* species. *PLoS ONE* **12**, e0185830 (2017).
96. Reithofer, M. & Jahn-Schmid, B. Allergens with Protease Activity from House Dust Mites. *IJMS* **18**, 1368 (2017).
97. Weghofer, M. *et al.* Comparison of purified *Dermatophagoides pteronyssinus* allergens and extract by two-dimensional immunoblotting and quantitative immunoglobulin E inhibitions. *Clin Experimental Allergy* **35**, 1384–1391 (2005).
98. Thomas, W., Heinrich, T., Smith, W.-A. & Hales, B. Pyroglyphid House Dust Mite Allergens. *PPL* **14**, 943–953 (2007).
99. Meno, K. *et al.* The Crystal Structure of Recombinant proDer p 1, a Major House Dust Mite Proteolytic Allergen. *The Journal of Immunology* **175**, 3835–3845 (2005).
100. De Halleux, S. *et al.* Three-dimensional structure and IgE-binding properties of mature fully active Der p 1, a clinically relevant major allergen. *Journal of Allergy and Clinical Immunology* **117**, 571–576 (2006).
101. Chruszcz, M. *et al.* Crystal Structures of Mite Allergens Der f 1 and Der p 1 Reveal Differences in Surface-Exposed Residues that May Influence Antibody Binding. *Journal of Molecular Biology* **386**, 520–530 (2009).

102. Derewenda, U. *et al.* The Crystal Structure of a Major Dust Mite Allergen Der p 2, and its Biological Implications. *Journal of Molecular Biology* **318**, 189–197 (2002).
103. Park *et al.* Localization of a major allergen, Der p 2, in the gut and faecal pellets of *Dermatophagoides pteronyssinus*. *Clin Experimental Allergy* **30**, 1293–1297 (2000).
104. Ihrie, M. D. *et al.* STAT6-dependent exacerbation of house dust mite-induced allergic airway disease in mice by multi-walled carbon nanotubes. *NanoImpact* **22**, 100309 (2021).
105. Radauer-Preiml, I. *et al.* Nanoparticle-allergen interactions mediate human allergic responses: protein corona characterization and cellular responses. *Part Fibre Toxicol* **13**, 3 (2015).
106. Kuijpers, E. *et al.* Occupational Exposure to Multi-Walled Carbon Nanotubes During Commercial Production Synthesis and Handling. *ANNHYG* **60**, 305–317 (2016).
107. Nowack, B. *et al.* Potential release scenarios for carbon nanotubes used in composites. *Environment International* **59**, 1–11 (2013).
108. Schneider, C. A., Rasband, W. S. & Eliceiri, K. W. NIH Image to ImageJ: 25 years of image analysis. *Nat Methods* **9**, 671–675 (2012).
109. Cox, J. & Mann, M. MaxQuant enables high peptide identification rates, individualized p.p.b.-range mass accuracies and proteome-wide protein quantification. *Nat Biotechnol* **26**, 1367–1372 (2008).
110. Tyanova, S., Temu, T. & Cox, J. The MaxQuant computational platform for mass spectrometry-based shotgun proteomics. *Nat Protoc* **11**, 2301–2319 (2016).
111. cRAP protein sequences. The Global Proteome Machine (2012).
112. Tyanova, S. *et al.* The Perseus computational platform for comprehensive analysis of (prote)omics data. *Nat Methods* **13**, 731–740 (2016).
113. Perez-Riverol, Y. *et al.* The PRIDE database and related tools and resources in 2019: improving support for quantification data. *Nucleic Acids Research* **47**, D442–D450 (2019).
114. Ricardo Prada Silvy, Christophe Pirlot, & Benedicte Culot. Catalyst system for a multi-walled carbon nanotube production process. (2011).
115. Ricardo Prada Silvy, Fanny Liegeois, Benedicte Culot, & Stephanie Lambert. Method of synthesising a support catalyst for the production of carbon nanotubes. (2010).

116. Dupuis, A. The catalyst in the CCVD of carbon nanotubes—a review. *Progress in Materials Science* **50**, 929–961 (2005).
117. White, C. M., Banks, R., Hamerton, I. & Watts, J. F. Characterisation of commercially CVD grown multi-walled carbon nanotubes for paint applications. *Progress in Organic Coatings* **90**, 44–53 (2016).
118. Monopoli, M. P. *et al.* Physical–Chemical Aspects of Protein Corona: Relevance to *in Vitro* and *in Vivo* Biological Impacts of Nanoparticles. *J. Am. Chem. Soc.* **133**, 2525–2534 (2011).
119. Partikel, K. *et al.* Effect of nanoparticle size and PEGylation on the protein corona of PLGA nanoparticles. *European Journal of Pharmaceutics and Biopharmaceutics* **141**, 70–80 (2019).
120. Gräfe, C. *et al.* Intentional formation of a protein corona on nanoparticles: Serum concentration affects protein corona mass, surface charge, and nanoparticle–cell interaction. *The International Journal of Biochemistry & Cell Biology* **75**, 196–202 (2016).
121. Poulsen, K. M. & Payne, C. K. Concentration and composition of the protein corona as a function of incubation time and serum concentration: an automated approach to the protein corona. *Anal Bioanal Chem* **414**, 7265–7275 (2022).
122. Cyphert-Daly, J. M., Yang, Z., Ingram, J. L., Tighe, R. M. & Que, L. G. Physiologic response to chronic house dust mite exposure in mice is dependent on lot characteristics. *Journal of Allergy and Clinical Immunology* **144**, 1428-1432.e8 (2019).
123. G. M. Hilton. (Norht Carolina State University, 2017).
124. Runa, S., Hussey, M. & Payne, C. K. Nanoparticle–Cell Interactions: Relevance for Public Health. *J. Phys. Chem. B* **122**, 1009–1016 (2018).
125. Shannahan, J. The biocorona: a challenge for the biomedical application of nanoparticles. *Nanotechnology Reviews* **6**, 345–353 (2017).
126. Ihrie, M. D. *et al.* Inhalation exposure to multi-walled carbon nanotubes alters the pulmonary allergic response of mice to house dust mite allergen. *Inhalation Toxicology* **31**, 192–202 (2019).
127. Kurt, O. K., Zhang, J. & Pinkerton, K. E. Pulmonary health effects of air pollution: *Current Opinion in Pulmonary Medicine* **22**, 138–143 (2016).

128. Reid, C. E. *et al.* Critical Review of Health Impacts of Wildfire Smoke Exposure. *Environ Health Perspect* **124**, 1334–1343 (2016).
129. Reithofer, M. & Jahn-Schmid, B. Allergens with Protease Activity from House Dust Mites. *IJMS* **18**, 1368 (2017).
130. Nguyen, V. H. & Lee, B.-J. Protein corona: a new approach for nanomedicine design. *IJN Volume* **12**, 3137–3151 (2017).
131. Bilal, M., Qamar, S. A., Carballares, D., Berenguer-Murcia, Á. & Fernandez-Lafuente, R. Proteases immobilized on nanomaterials for biocatalytic, environmental and biomedical applications: Advantages and drawbacks. *Biotechnology Advances* **70**, 108304 (2024).
132. Arsalan, A. & Younus, H. Enzymes and nanoparticles: Modulation of enzymatic activity via nanoparticles. *International Journal of Biological Macromolecules* **118**, 1833–1847 (2018).
133. Bhattacharya, A., Pandit, S., Lee, S., Ebrahimi, S. B. & Samanta, D. Modulating Enzyme Activity using Engineered Nanomaterials. *ChemBioChem* e202400520 (2024) doi:10.1002/cbic.202400520.
134. Talbert, J. N. & Goddard, J. M. Enzymes on material surfaces. *Colloids and Surfaces B: Biointerfaces* **93**, 8–19 (2012).
135. Sheldon, R. A. Enzyme Immobilization: The Quest for Optimum Performance. *Adv Synth Catal* **349**, 1289–1307 (2007).
136. Díaz, J. F. & Balkus, K. J. Enzyme immobilization in MCM-41 molecular sieve. *Journal of Molecular Catalysis B: Enzymatic* **2**, 115–126 (1996).
137. Lee, C.-H., Lin, T.-S. & Mou, C.-Y. Mesoporous materials for encapsulating enzymes. *Nano Today* **4**, 165–179 (2009).
138. Piccinno, F., Gottschalk, F., Seeger, S. & Nowack, B. Industrial production quantities and uses of ten engineered nanomaterials in Europe and the world. *J Nanopart Res* **14**, 1109 (2012).
139. Flores-Cervantes, D. X., Maes, H. M., Schäffer, A., Hollender, J. & Kohler, H.-P. E. Slow Biotransformation of Carbon Nanotubes by Horseradish Peroxidase. *Environ. Sci. Technol.* **48**, 4826–4834 (2014).
140. Allen, B. L. *et al.* Mechanistic Investigations of Horseradish Peroxidase-Catalyzed Degradation of Single-Walled Carbon Nanotubes. *J. Am. Chem. Soc.* **131**, 17194–17205 (2009).

141. Zhao, Y., Allen, B. L. & Star, A. Enzymatic Degradation of Multiwalled Carbon Nanotubes. *J. Phys. Chem. A* **115**, 9536–9544 (2011).
142. Jun, L. Y. *et al.* Immobilization of Peroxidase on Functionalized MWCNTs-Buckypaper/Polyvinyl alcohol Nanocomposite Membrane. *Sci Rep* **9**, 2215 (2019).
143. Dominguez, J. *et al.* House dust mite extract forms a der p 2 corona on multi-walled carbon nanotubes: implications for allergic airway disease. *Environ. Sci.: Nano* **11**, 324–335 (2024).
144. Post, S. *et al.* The composition of house dust mite is critical for mucosal barrier dysfunction and allergic sensitisation. *Thorax* **67**, 488–495 (2012).
146. Kalsheker, N. A. *et al.* The House Dust Mite Allergen Der p1 Catalytically Inactivates α 1-Antitrypsin by Specific Reactive Centre Loop Cleavage: A Mechanism That Promotes Airway Inflammation and Asthma. *Biochemical and Biophysical Research Communications* **221**, 59–61 (1996).
147. Reginald, K. & Chew, F. T. The major allergen Der p 2 is a cholesterol binding protein. *Sci Rep* **9**, 1556 (2019).
148. De Paoli, S. H. *et al.* The effect of protein corona composition on the interaction of carbon nanotubes with human blood platelets. *Biomaterials* **35**, 6182–6194 (2014).
149. Chen, M., Zeng, G., Xu, P., Lai, C. & Tang, L. How Do Enzymes ‘Meet’ Nanoparticles and Nanomaterials? *Trends in Biochemical Sciences* **42**, 914–930 (2017).
150. Van Den Boom, J. *et al.* The other side of the corona: nanoparticles inhibit the protease taspase1 in a size-dependent manner. *Nanoscale* **12**, 19093–19103 (2020).
151. Zhang, C., Luo, S. & Chen, W. Activity of catalase adsorbed to carbon nanotubes: Effects of carbon nanotube surface properties. *Talanta* **113**, 142–147 (2013).
152. Wang, Y. *et al.* Formation of Protein Corona on Nanoparticles with Digestive Enzymes in Simulated Gastrointestinal Fluids. *J. Agric. Food Chem.* **67**, 2296–2306 (2019).
153. Drenth, J., Jansonius, J. N., Koekoek, R., Swen, H. M. & Wolthers, B. G. Structure of Papain. *Nature* **218**, 929–932 (1968).
154. Liu, C.-G., Desai, K. G. H., Chen, X.-G. & Park, H.-J. Preparation and Characterization of Nanoparticles Containing Trypsin Based on Hydrophobically Modified Chitosan. *J. Agric. Food Chem.* **53**, 1728–1733 (2005).

155. Nidhin, M., Ghosh, D., Yadav, H., Yadav, N. & Majumder, S. Structural and functional aspects of trypsin–gold nanoparticle interactions: An experimental investigation. *Materials Science and Engineering: B* **202**, 46–53 (2015).
156. Chapman, M. D. & Platts-Mills, T. A. Purification and characterization of the major allergen from *Dermatophagoides pteronyssinus*-antigen P1. *The Journal of Immunology* **125**, 587–592 (1980).
157. Chruszcz, M. *et al.* Crystal Structures of Mite Allergens Der f 1 and Der p 1 Reveal Differences in Surface-Exposed Residues that May Influence Antibody Binding. *Journal of Molecular Biology* **386**, 520–530 (2009).
158. Kalsheker, N. A. *et al.* The House Dust Mite Allergen Der p1 Catalytically Inactivates α 1-Antitrypsin by Specific Reactive Centre Loop Cleavage: A Mechanism That Promotes Airway Inflammation and Asthma. *Biochemical and Biophysical Research Communications* **221**, 59–61 (1996).
159. Hosseini, H. & Ghaffarzadeh, M. Surface functionalization of carbon nanotubes via plasma discharge: A review. *Inorganic Chemistry Communications* **138**, 109276 (2022).
160. Hou, P.-X., Liu, C. & Cheng, H.-M. Purification of carbon nanotubes. *Carbon* **46**, 2003–2025 (2008).
163. Nicoletti, M., Gambarotti, C. & Fasoli, E. Proteomic fingerprinting of protein corona formed on PEGylated multi-walled carbon nanotubes. *Journal of Chromatography B* **1163**, 122504 (2021).
164. Tenzer, S. *et al.* Rapid formation of plasma protein corona critically affects nanoparticle pathophysiology. *Nature Nanotech* **8**, 772–781 (2013).
166. Partikel, K., Korte, R., Mulac, D., Humpf, H.-U. & Langer, K. Serum type and concentration both affect the protein-corona composition of PLGA nanoparticles. *Beilstein J. Nanotechnol.* **10**, 1002–1015 (2019).
167. Zhang, T., Tang, M., Yao, Y., Ma, Y. & Pu, Y. MWCNT interactions with protein: surface-induced changes in protein adsorption and the impact of protein corona on cellular uptake and cytotoxicity. *IJN Volume* **14**, 993–1009 (2019).
168. Shannahan, J. H. *et al.* Comparison of Nanotube–Protein Corona Composition in Cell Culture Media. *Small* **9**, 2171–2181 (2013).
169. Hamilton, R. F., Wu, Z., Mitra, S., Shaw, P. K. & Holian, A. Effect of MWCNT size, carboxylation, and purification on in vitro and in vivo toxicity, inflammation and lung pathology. *Part Fibre Toxicol* **10**, 57 (2013).

170. Pearle, M. S., Calhoun, E. A., Curhan, G. C., & the UROLOGIC DISEASES OF AMERICA PROJECT. UROLOGIC DISEASES IN AMERICA PROJECT: UROLITHIASIS. *Journal of Urology* **173**, 848–857 (2005).
171. Alelign, T. & Petros, B. Kidney Stone Disease: An Update on Current Concepts. *Advances in Urology* **2018**, 1–12 (2018).
172. Coe, F. L. Kidney stone disease. *Journal of Clinical Investigation* **115**, 2598–2608 (2005).
173. Thongprayoon, C., Krambeck, A. E. & Rule, A. D. Determining the true burden of kidney stone disease. *Nat Rev Nephrol* **16**, 736–746 (2020).
174. Khan, S. R. *et al.* Kidney stones. *Nat Rev Dis Primers* **2**, 16008 (2016).
175. Perez Castro, E. *et al.* Differences in Ureteroscopic Stone Treatment and Outcomes for Distal, Mid-, Proximal, or Multiple Ureteral Locations: The Clinical Research Office of the Endourological Society Ureteroscopy Global Study. *European Urology* **66**, 102–109 (2014).
176. Ventimiglia, E. *et al.* High- and Low-Power Laser Lithotripsy Achieves Similar Results: A Systematic Review and Meta-Analysis of Available Clinical Series. *Journal of Endourology* **35**, 1146–1152 (2021).
177. Keller, E. X. *et al.* Fragments and dust after Holmium laser lithotripsy with or without “Moses technology”: How are they different? *Journal of Biophotonics* **12**, e201800227 (2019).
178. Kronenberg, P. & Traxer, O. The Truth About Laser Fiber Diameters. *Urology* **84**, 1301–1307 (2014).
179. Kronenberg, P. & Traxer, O. Update on lasers in urology 2014: current assessment on holmium:yttrium–aluminum–garnet (Ho:YAG) laser lithotripter settings and laser fibers. *World J Urol* **33**, 463–469 (2015).
180. Emiliani, E. *et al.* The True Ablation Effect of Holmium YAG Laser on Soft Tissue. *Journal of Endourology* **32**, 230–235 (2018).
181. Gilling, P. J., Cass, C. B., Cresswell, M. D. & Fraundorfer, M. R. Holmium laser resection of the prostate: Preliminary results of a new method for the treatment of benign prostatic hyperplasia. *Urology* **47**, 48–51 (1996).
182. Maxwell, A. D. *et al.* Simulation of Laser Lithotripsy-Induced Heating in the Urinary Tract. *Journal of Endourology* **33**, 113–119 (2019).

183. Teng, J. *et al.* Temperature profiles of calyceal irrigation fluids during flexible ureteroscopic Ho:YAG laser lithotripsy. *Int Urol Nephrol* **53**, 415–419 (2021).
184. Rezakahn Khajeh, N., Hall, T. L., Ghani, K. R. & Roberts, W. W. Pelvicaliceal Volume and Fluid Temperature Elevation During Laser Lithotripsy. *Journal of Endourology* **36**, 22–28 (2022).
185. Kim, J. S. *et al.* Indium–tin oxide treatments for single- and double-layer polymeric light-emitting diodes: The relation between the anode physical, chemical, and morphological properties and the device performance. *Journal of Applied Physics* **84**, 6859–6870 (1998).
186. Cirpan, A. & Karasz, F. E. Indium tin oxide nanoparticles as anode for light-emitting diodes. *J of Applied Polymer Sci* **99**, 3125–3129 (2006).

8. Biography

Judith Dominguez earned a Bachelor of Mechanical Engineering from the University of Minnesota Twin Cities in 2020. While earning her bachelor's degree, Judith worked as an undergraduate researcher in the BioSensing and BioRobotic Lab. This experience allowed her to apply to the National Science Foundation Graduate Research Fellowship Program (NSF GRFP) during her last year. Judith was awarded the NSF GRFP and Alfred F. Sloan Fellowship and began her PhD at Duke University in the Payne Lab. In her time at the Payne Lab, Judith primarily worked on characterizing protein coronas on MWCNTs, as a part of a collaboration with the Bonner Lab at North Carolina State University. She also joined a new project aimed to develop a new procedure for laser lithotripsy in which a nanofluid would be used to reduce thermal damage to tissues. This project was collaboration between all professors, graduate students, postdoctoral associates, and urologists that form a part of the P20 group. Her research was supported under the National Institute of Health Supplement to Promote Diversity in Health-Related Research award. In addition to research, Judith was Graduate Student Representative in Duke's Society of Hispanic Professional Engineers chapter.